Evaluating terrain-based HAND-SRC flood mapping model in low-relief rural plains using high resolution topography and crowdsourced data

Hassan Sabeh, Chadi Abdallah, Nanée Chahinian, Marie-George Tournoud, Rouya Hdeib, Roger Moussa

Journal Pre-proofs

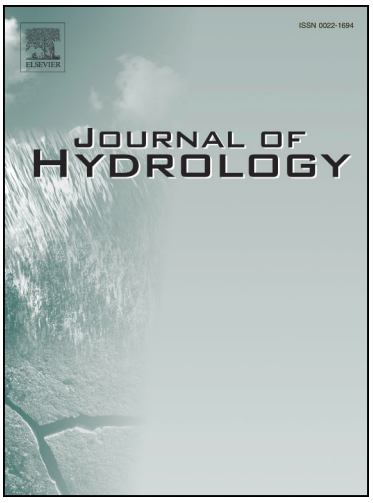

Research papers

Evaluating terrain-based HAND-SRC flood mapping model in low-relief rural plains using high resolution topography and crowdsourced data

Hassan Sabeh, Chadi Abdallah, Nanée Chahinian, Marie-George Tournoud, Rouya Hdeib, Roger Moussa

PII: S0022-1694(24)02045-6
DOI: https://doi.org/10.1016/j.jhydrol.2024.132649
Reference: HYDROL 132649

To appear in: *Journal of Hydrology*

Received Date: 17 July 2024
Revised Date: 5 December 2024
Accepted Date: 9 December 2024

Please cite this article as: Sabeh, H., Abdallah, C., Chahinian, N., Tournoud, M-G., Hdeib, R., Moussa, R., Evaluating terrain-based HAND-SRC flood mapping model in low-relief rural plains using high resolution topography and crowdsourced data, *Journal of Hydrology* (2024), doi: https://doi.org/10.1016/j.jhydrol.2024.132649

Evaluating Terrain-Based HAND-SRC Flood Mapping Model in Low-Relief Rural Plains Using High Resolution Topography and Crowdsourced Data

Keywords:

Height above nearest drainage; Synthetic rating curve; Low-complexity model; DEM resolution; Hydro-conditioning; HEC RAS

Authors and affiliations:

Hassan Sabeh[a,b,*], Chadi Abdallah[a], Nanée Chahinian[b] , Marie-George Tournoud[b], Rouya Hdeib[c], Roger Moussa[d]

[a] *National Center for Natural Hazards and Early Warning, CNRS-L, Beirut, Lebanon*

[b] *HSM Montpellier, Univ Montpellier, CNRS, IRD, Montpellier, France*

[c] *Department of Civil and Architectural Engineering, Applied Science University, Manama, Kingdom of Bahrain*

[d] *LISAH, Univ Montpellier, INRAE, IRD, Institut Agro, Montpellier, France*

* *Corresponding author*

E-mail address: hassan.sabea@cnrs.edu.lb

Abstract

Low-complexity terrain-based models are increasingly utilized for their rapid simulation time and low data requirements. The Height Above Nearest Drainage terrain index coupled with Synthetic Rating

Curves (HAND-SRC) emerges as a prominent model for mapping floods from a digital elevation model (DEM). However, the DEM requirements for its implementation remain unclear in many geographic settings. In this study, we evaluate the terrain conditions necessary for HAND-SRC flood mapping in rural low-relief terrain. This was investigated in the Ostouane River, Northern Lebanon, where an intensive field investigation was conducted to collect a high-resolution DEM (25 cm), bathymetric cross-sections, and a crowdsourced dataset reconstituting the January 2019 flood event. Specifically, we scrutinize both the terrain's geometric representation and its resolution. An adapted hydro-conditioning process was introduced to assess flood mapping performance. This process integrated surveyed and theoretical bathymetry, enforced drainage into both bathymetry and floodplain and removed levees in an unorthodox approach. The generated terrain was then tested after resampling it into coarser DEM resolutions. The hydro-conditioned terrain with integrated surveyed bathymetry demonstrated reliable flood mapping accuracy against crowdsourced data (CSI = 0.64 and RMSE = 0.54 m) and HEC-RAS extents (CSI = 0.66). Introducing a theoretical trapezoidal bathymetry based on hydraulic geometry power laws produced improved metrics due to enhanced drainage continuity between the channel and floodplains. Analysis of the resampled terrains highlights a random loss of terrain convergence and geometric accuracy, disrupting the model's implementation and accuracy at coarser resolutions (> 1 m). Overall, the comprehensive hydro-conditioning approach allows the model to depict the full inundation extent and retain the topographic accuracy in the HAND index raster. A sufficient grid resolution that maintains terrain convergence and drainage continuity is essential to overcome the challenges of low-relief topography. While the model admits limitations in cell-by-cell flood depth estimations, we suggest that it can be highly beneficial for rapid and accurate flood mapping.

1. Introduction

Floods are one of the most threatening natural hazards, imposing significant risk on exposed populations. Every year, around 83 million humans are impacted by floods, causing billions of dollars in losses and thousands of casualties (CRED, 2022; Rentschler & Salhab, 2020). Driven by the need for comprehensive flood risk management, floods have become a major focus of scientific research aimed at improving methods that facilitate hazard modelling, inundation mapping and emergency response (Jafarzadegan et al., 2023; Teng et al., 2017).

The distinctive flooding problems encountered in various basins worldwide triggered the synthesis of a multitude of adapted modelling techniques during the past decades. Yet, finding an approach that best fits the modelling problem and purpose is still a challenge in the field (Jafarzadegan et al., 2023). Factors such as data availability, flood response time, computational requirements, basin characteristics and the desired level of accuracy define these problems and dictate the choice and complexity of the approach. The availability and reliability of gauged rainfall and discharge data needed for model optimization, remain a major concern in ungauged and data-scarce basins around the globe (Grimaldi et al., 2013). Nevertheless, the integration of remote sensing and crowdsourcing as alternative sources of information has contributed to improving modelling accuracy despite their constraints in temporal domains (Notti et al., 2018; Sy et al., 2019). Topographic data remain the main input in any type of flood modelling and have become highly accessible providing extensive coverage at global scale. Simultaneously, topographic surveying techniques can now provide accurate, high resolution and low-cost products (Tamminga et al., 2015). This transformation and expansion in input data, be it in quality, quantity, scale or coverage presents an opportunity to assess new generations of well adapted inundation mapping approaches.

In general, three classifications of flood mapping methods can be identified: empirical methods, hydraulic models, and simplified conceptual methods (Teng et al., 2017). Empirical methods directly rely on statistical approaches and on observational data (Mudashiru et al., 2021). However, they can be limited in their spatio-temporal domains and constrained by engineering, financial and environmental factors. Hydraulic models are the most utilized approach for replicating flow dynamics based on shallow water

equations. They require many inputs, including channel and floodplain geometries, surface roughness coefficients and hydraulic structures dimensions, necessitating substantial computational resources. In contrast, simplified conceptual models, also referred to as "low-complexity models", adopt simplified physical concepts that rely mainly on topographic information for flood delineation. Many of these models are based on the manipulation and analysis of digital elevation models (DEMs) through various techniques such as filling and spilling (Lhomme et al., 2008; Jafarzadegan et al., 2023) or by integrating power laws of hydraulic geometry such as the hydro-geomorphic method and the geomorphic flood index method (Annis et al., 2019; Deiana et al., 2023; Nardi et al., 2006). These models have become more prominent driven by the advantages they offer despite lacking accurate representation of overland flow physics (Afshari et al., 2018; Dhote et al., 2023; McGrath et al., 2018).

Terrain based flood mapping approaches were initially driven by the widespread availability of satellite-based DEMs covering many ungauged basins around the globe. The concept behind their development asserts that floodplains can be distinguished relying on the geomorphic footprint that remains embedded in the terrain even in altered and urbanized areas (Annis et al., 2019; Nardi et al., 2006). This has led to the emergence of several terrain-based models that extract the topographic properties of rivers and floodplains in the form of synthetic and composite indices (Lioi et al., 2020) such as the geomorphic flood index (Samela et al., 2017), the topographic index (Beven & Kirkby, 1979; Manfreda et al., 2011) and slope position (Dhote et al., 2023). Because of their low-complexity, low data requirement and rapid simulation time, these methods have been adopted for flood forecasting and large-scale flood inundation mapping. Despite that, their accuracy has been hampered by the coarse resolutions of DEMs (Manfreda et al., 2014), which are unable to capture flood controlling features (Schumann et al., 2013). However, the increasing availability of high-resolution digital elevation models (HRDEM) may provide new avenues in this field as they have undeniable advantages in terms of vertical accuracy and detection of detailed features. Finer resolutions were found to improve the performance in low-complexity terrain-based approaches (Aristizabal et al., 2024; Garousi-Nejad et al., 2019). However, such level of detail can introduce additional errors and require supplementary processing caused by artificial structures and topographic depressions that influence the flow direction and accumulation patterns especially in complex low-relief terrains (Woodrow et al., 2016; Zheng et al., 2018a). Furthermore, terrain representation within a DEM is another concern in flood modelling. Features such as bathymetry and levees are critical components that influence the performance and accuracy of various models (Afshari et al., 2018; Ghanghas et al., 2022; Wing et al., 2019a).

Height Above Nearest Drainage or HAND is a terrain index defined as the height of a DEM grid cell above the nearest drainage flow line into which the cell drains. The concept of HAND was first introduced by Rennó et al. (2008) based on initial attempts by Rodda (2005) to map floods on a cell-by-cell basis. The approach utilizing HAND index use a stage height representing a water level above a reference drainage line. Subsequently, all DEM grid cells hydrologically connected to the drainage line are classified as either flooded or non-flooded cells based on the HAND value of each cell. The literature on HAND highlights several developments aimed at overcoming the limitations of the method. The main novelty in the approach is the introduction of synthetic rating curves (SRCs) by Zheng et al. (2018b), which allow estimating a stage height from normalized hydraulic geometry over a river reach. HAND-SRC as a parsimonious hypsometric model has shown to be reliable for flood inundation mapping when tested against established flood maps, gauged observations and remote sensing data (Aristizabal et al., 2024; Garousi-Nejad et al., 2019; Johnson et al., 2019; Zheng et al., 2018b). The National Water Center (NWC) in the US implemented the model for continental-scale flood inundation mapping and integrated it into operational forecasting (Li et al., 2023; Liu et al., 2018). Nevertheless, its applications extend to hydrological landscape classification (Gharari et al., 2011), detection of groundwater potential areas (Hamdani & Baali, 2019) and in correlating soil-water gradients (Schietti et al., 2014).

Within flood modelling domain, crowdsourced data has been increasingly integrated as it has emerged as a supplementary low-cost source of information. Such data are a product of the participatory contribution of the general public in generating and developing new knowledge that can be beneficial in a scientific context (Buytaert et al., 2014). The integration usually exploits photographic records, videos, texts and measurements collected through different means such as interviews, applications and social networks. Furthermore, it relies on eyewitness accounts to characterize and extract geo-tagged information on past flood events (Paul et al., 2018; Sy et al., 2019, 2020). Such observations have also been assimilated into hydrological and hydraulic models with the objective of enhancing flood forecasting (Mazzoleni et al., 2017; Songchon et al., 2023) or to calibrate and validate inundation models (Dasgupta et al., 2022; Gitundu et al., 2023; Malgwi et al., 2021). Crowdsourced data proves to be advantageous compared to satellite imagery by providing dense and detailed information of flood depths in urban settings. This data can be particularly useful in small ungauged basins whose flood response is faster than the satellite revisit interval.

Most recent research on the HAND-SRC flood hazard mapping scrutinized large scale applications, where coarse satellite-based DEMs enable the operational use of the model at regional and national scales (Liu et al., 2018; Yamazaki et al., 2019). Nevertheless, a comprehensive assessment of HAND-SRC at smaller scales is still very limited (Li et al., 2023) and its adaptation in different geographies remains scarce (Wing et al., 2019b). Furthermore, combining high resolution DEMs with bathymetric surveys is absent in the literature, while crowdsourced data remain largely untested for assessing terrain-based models (Zheng et al., 2022). Despite the advancements in the HAND-SRC approach, low-relief terrains have been found to present a challenge due to the inherent problems in the DEMs and the modelling implementation (Afshari et al., 2018; Godbout et al., 2019; Hocini et al., 2020; Jafarzadegan et al., 2022; Johnson et al., 2019). A literature review on HAND-SRC in low-relief regions revealed two key aspects that could potentially enhance the model's performance. These were: (1) the terrain setup, including feature representation and DEM preparation through hydro-conditioning and (2) the DEM resolution and accuracy.

The main objective of this study is to evaluate the conditions necessary for effective fluvial flood mapping using the HAND-SRC model in a low-relief setting. It also aims to assess the opportunities from using high-resolution DEM based on a series of tested configurations that scrutinize the terrain and its resolution. For this purpose, a high-resolution digital elevation model, a bathymetric survey, and a dataset of crowdsourced past flood water levels were utilized. The study was conducted in a low-relief rural floodplain with anthropogenic features, comprising a mixed urban and agricultural landscape within a small Mediterranean basin. This work encompasses an intensive field investigation to collect a detailed spatial and topographic dataset in addition to a crowdsourcing campaign of a past event.

The paper is divided into four sections. The first section describes the study area and its hydrological, morphometric and physical characteristics as well as the acquisition of the topographic, spatial, hydrometric and crowdsourced datasets. The second section presents the methodology followed to develop the HAND-SRC terrain-based model and a HEC RAS hydraulic model. The proposed steps for preparing the DEM by creating terrain setups are then outlined along with the parameters, resolutions and metrics used for evaluation. In the results section, the terrain hydro-conditioning processes and parameter choices are first evaluated, followed by the flood mapping performance and finally the effect of varying DEM resolution. Thereafter, the findings are discussed in light of the tested processes and configurations. Finally, conclusions are drawn on the capabilities and limitations of the HAND-SRC with recommendations for future work.

2. Study area and data

2.1. Ostouane basin in North Lebanon

The study is conducted in the Ostouane River basin located in Northern Lebanon in the region of Akkar (Fig. 1a). The basin is one of the country's coastal catchments along the eastern Mediterranean. The river's headwaters originate from the northernmost section of the Mount Lebanon range near Akkar al-Attika. The river drains an area of approximately 144.1 km^2 and flows in a western direction down to its estuary. The maximum altitude in the basin is 1923 meters, with an average land slope of 25.6%.

The basin has a Mediterranean climate, characterized by cool rainy winters and dry hot summers. The annual rainfall ranges from 667 mm/yr near the coast up to 1040 mm/yr over the high mountainous areas, with an average of 861 mm/yr. The average discharge of the river is 2.2 m^3/s, with a maximum monthly flow of 7.9 m^3/s during February. For a 100-year return period, a peak flow of 118.5 m^3/s is estimated at Pont Halba gauge station. However, the basin lacks reliable long-term precipitation records that can capture the intensity of sub-daily rainfall events. Despite the existence of three rainfall stations, issues such as recurrent failures, non-coinciding records and the absence of sub-daily measurements prevent a comprehensive hydrological assessment.

The basin's topography can be divided into a mountainous relief with steep regions on the eastern and central parts, and a flat floodplain terrain that is most susceptible to inundation near the estuary. The river's slope decreases from 2.09% near the headwaters to 0.08% as it flows into the Akkar Plain. Its average width varies between 8 and 12 meters along its course, widening up to 42m upstream of Kneisseh village. The river then flows into a series of meanders in a deep and narrow channel that varies between 6 and 10 meters in width, with low slope and densely vegetated banks.

The land cover in the basin is dominated by agricultural areas (44.2%), followed by wooded lands (26%), and urbanized areas (5%). The scrutinized rural floodplain (Fig. 1c & Figs. 2a,2b,2c) is mainly agricultural with dispersed urbanization, and is characterized by anthropogenic features such as canals, ditches and levees. These were developed to support local agricultural practices and for flood mitigation purposes. The levees present are small soil embankments individually developed by local farmers. They are not optimized or built per engineering standards, with gaps and breaches, and are scattered along different segments of the river.

According to the FAO-UNESCO soil classification system, the basin is primarily covered by Cambisols (30.9%), Leptosols (22.5%), and Luvisols (21.5%) (Darwish et al., 2006). Surface formations of the Ostouane basin include the Cenomanian-Turonian (C4-C5) limestone which consists of limestone, dolomites and marly limestone. This formation outcrops in the eastern part of the basin (41.1%) and is the main contributor of spring discharge. A Pliocene basalt formation outcrops in the central and western regions of the basin (42.7%) whereas a Holocene formation of silt, sand and fluvial gravel covers the floodplain of the river (Dubertret, 1945). Moreover, several aquifer formations underly the basin, including the North Lebanon Cretaceous, Qammoua Cretaceous and the Akkar Neogene-Quaternary aquifers. The last two are separated by an unproductive Basalt aquiclude.

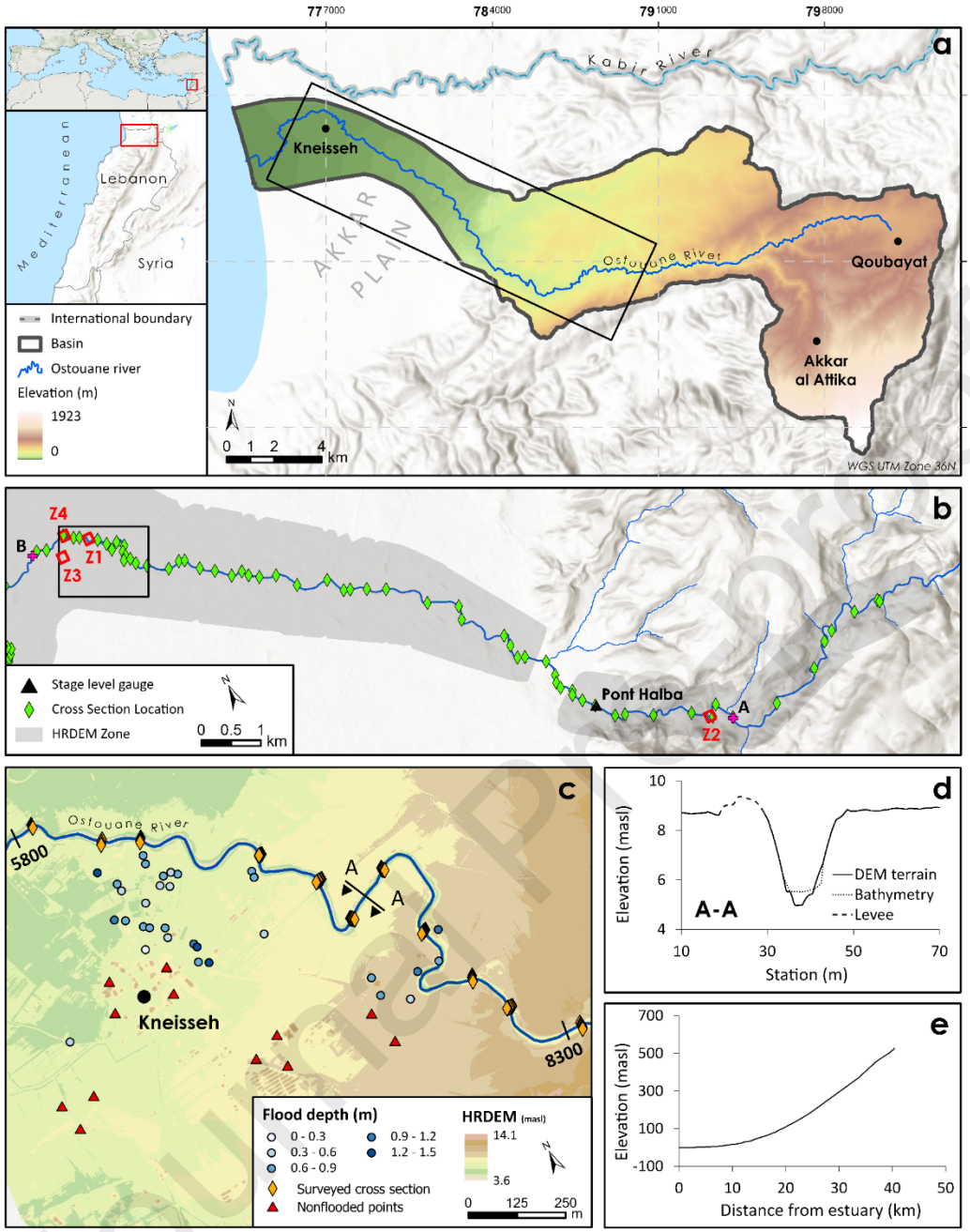

Figure 1: (a) Location of the Ostouane basin on the eastern Mediterranean in northern Lebanon showing elevation, main river course and significant towns; (b) extent of the high-resolution DEM (HRDEM) where the HAND-SRC model was implemented, the extent of HEC RAS model implementation (A-B), location of the Pont Halba river gauge station, and zones Z1, Z2, Z3 and Z4; (c) test site showing crowdsourced flood depths, locations of non-flooded point, surveyed cross-section points, and cross-section A-A; (d) cross-section profile A-A showing the original terrain, surveyed bathymetry and levee and (e) constructed longitudinal profile of the Ostouane river from surveyed cross-sections

2.2. Data acquisition

An intensive field investigation was conducted along the floodplains of the study area. This section describes the methods and tools used to acquire and develop the input datasets. A summary description of the collected datasets is shown in Table 1.

2.2.1. High-resolution digital elevation model (HRDEM)

A high-resolution digital elevation model (HRDEM) was produced using a fixed-wing drone photogrammetry over an area of 21.6 km^2 along the river floodplains (Fig. 1b). The process consisted in capturing a series of around 18,000 overlapping photos from which a 3D point cloud was generated. The point cloud derived from the Structure from Motion (SfM) technique was then transformed into space coordinates based on ground control points (GCPs) (Westoby et al., 2012). The digital terrain model was then processed by clearing all surfaces above the natural ground. The final resolutions of the DEM parts generated along different segments of the floodplains ranged between 10 and 20 cm. In order to standardize the resolution, all DEM parts were resampled using bilinear interpolation to a 25 cm resolution. One part of HRDEM was disregarded due to high vertical error resulting in two separate sub-parts. The interpolated DEM is denoted HRDEM in this study. A vertical accuracy assessment was conducted using a set of 19 ground truth points surveyed using an RTK GPS over the HRDEM of the study zone. The assessment showed a mean absolute error (MAE) of 3.4 cm and a root mean square error (RMSE) of 21.3cm. These values fall within the reported range of error in drone photogrammetry DEMs (Greenwood et al., 2019; Siebert & Teizer, 2014).

2.2.2. River bathymetry

The geometric data of the river channel were extracted through a series of cross-sections surveyed using a dual frequency RTK GPS (Fig. 2d). The spacing between consecutive cross sections was 220 meters on average, with a maximum spacing of 400 meters. A total of 58 collected cross-sections were utilized within the modelling domain (Fig. 1b). Figure 1d displays an example of a surveyed cross-section compared to the bathymetry of the DEM. The longitudinal profile of the river constructed using the surveyed cross sections is shown in figure 1e.

2.2.3. Land use data

The land cover dataset is based on digitizing GeoEye (2021) high-resolution imagery on a scale of 1/5000 over the catchment and a 1/1000 scale within the floodplains (Abdallah et al., 2023). The land use/land cover corresponds to 34 different classes based on CORINE land classification adapted for Lebanon.

2.2.4. River stage data

Gauged water levels at the Pont Halba station and flow records were obtained from the Lebanese Litani River Authority. The gauge is located at an elevation of 76 masl and controls a draining area of 100 km^2. The measurements are automated at a 15 or 45-minute interval. However, the flow records provided by the authority are of average daily discharge values. The stage-discharge relationship developed by LRA at the site relies on scarce in-situ flow measurements. During high flow conditions, these measurements are unavailable inducing large errors caused by the mere extrapolation of the rating curve. To address this, a theoretical rating curve was established using the topographic dataset and calibrated against the daily discharge. The rating curve was then used to convert the gauged water levels into more refined sub-daily flow estimates. The peak discharge of the January 2019 flood event was then estimated as Q_p=94.1 m^3/s at Pont Halba station.

2.2.5. Crowdsourcing data on 2019 flood event

The crowdsourcing of the past flood event was conducted in a similar approach to that of Sy et al. (2020). Due to the lack of an official census on flood events, the crowdsourcing campaign was conducted in 2023 to collect eyewitness accounts and observations of past events at the flood impact locations. The most intense flood within the past 5 years, namely that of the 7th of January 2019 was scrutinized. The flood resulted in the inundation of both banks and the devastation of vast agricultural land and houses. The investigation targeted the inhabitants of this flood zone.

The main challenge faced during crowdsourcing inquiries is the elapsed time between the survey date and the flood event. Relying on eyewitness memory retrievals in describing flood events can induce uncertainties caused by memory distortions especially when a long time has passed since the event (Lacy & Stark, 2013). To minimize the impact of such distortion, the survey consisted of two phases. The first phase involved helping eyewitnesses recall the exact event by communicating the date, time, description, impact and proceedings of that event. The second phase included extracting observations by asking about the witnessed flood levels and extent. The enquiring of flood levels was repeated in a suggestive manner, with the respondents being asked to refer to a fixed object or a body part. Two coordinate points were then collected using a high-accuracy RTK GPS device: the maximum witnessed flood water elevation and the ground elevation below. Points that showed a significant error between the measured ground level in comparison to the DEM terrain levels were filtered out. Such discrepancies emerged from measurement errors or dense vegetation cover affecting the vertical accuracy of the DEM at a given location.

The final dataset comprised 33 peak flood levels and 12 non-flooded points. The average difference between the riverbed profile and the elevation of the crowdsourced flood points was 3.93 m. The vertical error between the HRDEM and the terrain elevation collected at the location of the crowdsourced flood depth measurements showed a MAE of 14.07 cm and a RMSE of 16.68 cm. The similar values of MAE and RMSE indicate a uniform distribution of error values. The majority of crowdsourced data were collected on the left bank of the Ostouane River where most houses and observations are found (Fig. 1c). Finally, a flood map was delineated using the collected extent and interpolated flood elevation points (Fig. SM1 in supplementary material).

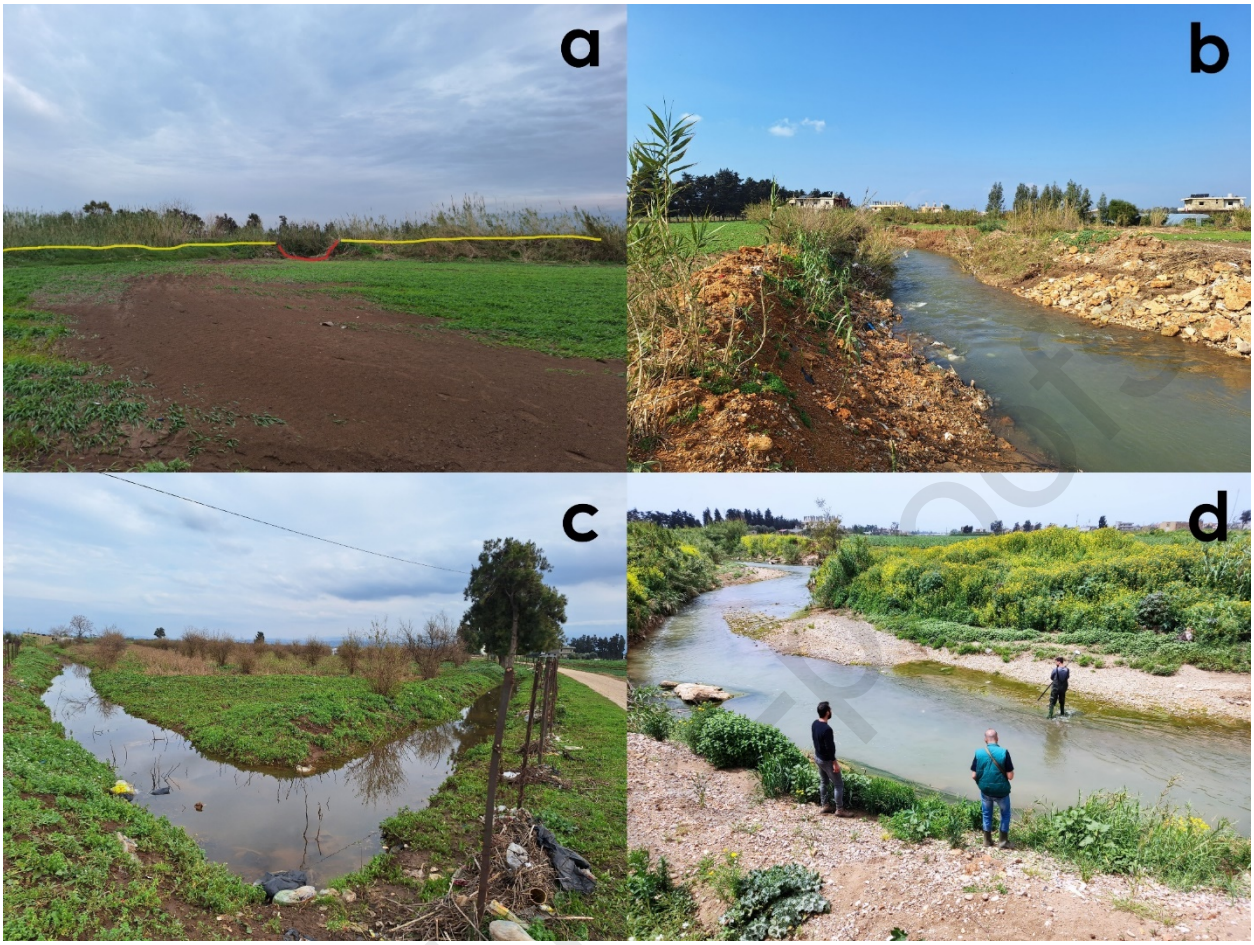

Figure 2: Photos from field survey at Ostouane river: (a) a small breached levee developed by locals, (b) river channel next to a non-engineered levee on one side, (c) ditches found around the agricultural lands in the floodplain, and (d) river bathymetry survey

Table 1. Summary of surveyed, collected and developed datasets

Dataset	Source	Description/location	Scale/Resolution
Digital elevation model (DEM)	Drone Photogrammetry	DEM of floodplain	25 cm
Cross sections	Bathymetry survey	58 bathymetry cross sections	-
Land Use and Cover (LUC)	GeoEye (2020)	Digitized map with 35 classes	1/1000

River stage	Litani River Authority (LRA)	Pont Halba station	15 min
River flow	Litani River Authority (LRA)	Pont Halba station	daily
Crowdsourced flood levels	Field investigation	34 water levels & terrain elevation	-
Crowdsourced non-flooded locations	Field investigation	12 non-flooded points	-

3. Methodology

A terrain-based HAND-SRC model and a hydraulic-based HEC RAS model were developed here to assess the performance of the former. This section describes (1) the implementation of the HAND-SRC model, (2) the implementation of the HEC RAS model, (3) the approach and metrics used to evaluate flood mapping, and (4) the workflow of the study.

3.1. Terrain-based flood mapping: HAND-SRC

The HAND-SRC model was implemented in two sub-parts of the study area, with areas of 15 and 6.6 km^2 of the HRDEM (Fig. 1b).

3.1.1. Model overview

The implementation of HAND-SRC for flood mapping (fig. SM2 in supplementary material) consists of three main steps: (a) calculation of the HAND raster, (b) extraction of hydraulic geometry and plotting SRCs for each catchment and (c) flood mapping. The general approach adopted for the calculation of the HAND raster and plotting of SRCs is similar to that found in previous literature (Aristizabal et al., 2023; Garousi-Nejad et al., 2019; Zheng et al., 2018a, 2018b).

a. HAND raster

The HAND raster represents a grid of HAND index values denoted *H*. The index signifies the hypsometric position of each DEM grid cell relative to a hydrologically connected reference drainage line, denoted in this work as "flowline". The HAND index value is calculated as the elevation difference between the DEM grid cell and the flowline grid cell (Eq. 1).

$$H = elevation_{DEM\ grid\ cell} - elevation_{connected\ flowline\ grid\ cell} \quad (1)$$

The HAND raster grid is computed in five steps: (1) the river flowline is rasterized to match the grid size of the DEM, (2) the pits are removed from the DEM using the *PitRemove* utility of TauDEM software (Tarboton, 2024), (3) the D-infinity (D_∞) multiple flow direction model and the slope raster are calculated using *DinfFlowDir* utility. Finally, (4) the HAND raster is generated using D-infinity distance down *DinfDistDown* utility which provides *H* values referenced to the flowline.

b. Hydraulic geometry and SRCs for a catchment

A catchment is defined hereafter as an area draining into a specific river reach of length L, that is a parameter in the HAND-SRC model. The catchment's hydraulic geometry for a given L is computed from the HAND raster using predefined stage heights h. The process involves hypothetically filling the raster up to a given stage height h and comprises the following six steps: (1) the flowline is discretized into a set of reaches according to the reach length L, (2) the reaches are rasterized, (3) the catchment of each reach is delineated using GRASS GIS *r.stream.basins* utility, (4) attributes of each reach (ID, slope, length and area) are assigned to their corresponding catchment, (5) the reach scale hydraulic geometry (flood volume V, inundated surface area F, wetted riverbed area B, slope S) are calculated using *catchhydrogeo* utility of TauDEM, (6) these geometries are normalized against L to derive the wetted cross-sectional area A, top width T, wetted perimeter P, and hydraulic radius R. Finally, a discharge (Q) corresponding to a catchment of a reach length L, at a stage height h, is determined using Manning's flow equation (Eq. 2):

$$Q_{(h)} = \frac{1}{n} A_{(h)}^{2/3} R_{(h)}^{1/2} = \frac{1 V_{(h)}^{5/3} S^{1/2}}{n \quad LB_{(h)}} \qquad (2)$$

Manning's roughness coefficient n is the other parameter of the HAND-SRC model. For a fixed value of n, the calculation of the Q is repeated for each height h using Python™ scripts, which allow to plot a synthetic rating curve (SRC) for each catchment.

c. Mapping flooding areas and flood depths

For a simulated discharge Q, a stage height h is extracted from the SRC at each catchment. This stage height is used to generate flood inundation maps through binary classification (inundated vs. not inundated) based on the HAND index values H. The stage height h is the HAND-SRC model variable.

The flood mapping is carried out by (1) denoting all grid cells with H value greater than h as non-flooded, and (2) assigning the flood inundation depth as the difference between the H value at a grid cell and h at its corresponding catchment (*depth=h-H)*. This procedure was performed using ArcHydro tools.

3.1.2. Model assumptions

The implementation of the HAND-SRC model requires conforming to five key assumptions. These are: (A1) All DEM grid cells susceptible to inundation must drain into the flowline. (A2) Within a processing region the drainage must flow into a unique outlet. (A3) The stage height h is uniformly applied across each catchment. (A4) Catchments are independent meaning no flow or volume exchange occurs at the catchment boundaries. (A5) The filling volume is infinite. The first two assumptions (A1 and A2) necessitate a hydro-conditioning process of the underlying terrain to: (a) enforce the drainage of flood-prone areas into the river channel and (b) ensure a continuous decrease in elevations along the drainage network and the flowline toward the outlet. Since DEMs do not necessarily adhere to these assumptions, errors may arise from these processes depending on the region and methods used. The last three assumptions (A3, A4 and A5) govern the application of stage height h, which may introduce errors and limitations in the model.

3.1.3. Hydro-conditioning and definition of terrain setups

Hydro-conditioning of the HRDEM was applied over the whole modelling domain prior to the implementation of the HAND-SRC model. The hydro-conditioning processes account for the features controlling the flooding processes while adhering to the model assumptions. Additionally, these processes aim to mitigate and limit the impact of the inaccuracies resulting from the automatic HAND raster

calculation process (section 3.1.1) on terrain accuracy. Three types of hydro-conditioning are introduced here: (a) integration of riverbed bathymetry, (b) enforcement of the floodplain drainage system, and (c) removal of levees.

a. Integration of river bathymetry

Riverbed bathymetry was integrated into the 25-cm HRDEM, incorporating either: (1) the surveyed bathymetry, after an interpolation process or (2) a hypothetical trapezoidal cross-sectional shaped bathymetry, based on hydraulic geometry power laws. In both cases, the bathymetric DEMs were resampled into the 25-cm resolution and superimposed onto the HRDEM using ArcGIS Pro.

In the first case, the surveyed bathymetry was extracted from consecutive cross-sections through a curvilinear interpolation along the river talweg. The interpolation is based on a string model that connects successive cross-sections (USACE, 2020). To overcome the model's limitations in interpolating floodplains and discontinuities in bank boundaries (Merwade et al., 2008), the interpolation boundary was confined to the bathymetry zone delineated from drone imagery (Fig. SM3 in supplementary material). This interpolation used cross-sections at 50-meter intervals. Three major cords connected both banks and the minimum elevations of successive cross-sections, while minor cords connected the remaining points.

In the second case, the trapezoidal cross-section bathymetry was generated based on the local slope bounded by the river width and the upstream and downstream cross-sections. Based on channel survey, the cross-section geometry adopted a 1:2 ratio of horizontal to vertical side slopes. The top width of the riverbed was then extracted from drone imagery along the river course. The depth D of the riverbed was estimated from a power law expression of the top width W (Eq. 3) assuming a constant discharge at the capture time:

$$D = \alpha W^{\beta} \quad (3)$$

Regression of the surveyed bathymetric data resulted in values $\alpha = 0.7609$ and $\beta = -0.386$.

After integrating the bathymetry into the HRDEM, an additional process was needed to ensure the HRDEM adhere to the assumptions (A1) and (A2) of the model by enforcing a flowline in the bathymetry (see section 3.1.2). The flowline is essential for HAND inundation mapping as it serves as a reference for all HAND index calculations and is highly sensitive in low-slope rivers. To achieve a monotonically decreasing flowline, the following method was applied: (1) drainage within the bathymetry DEM was delineated based on the D8 flow accumulation grid (Lindsay, 2016). (2) The extracted flowline was then burned into the original DEM using the AGREE-DEM method (Hellweger, 1997) which excavates the DEM at the location of the flowline. Finally, (3) a fill-burn approach was applied to eliminate all bathymetric inconsistencies, errors and multiple flowlines within the river bed. The "fillburn" tool of WhiteboxTools was utilized (Lindsay, 2016; Saunders, 1999). This process enforced the flowline in the bathymetry while maintaining a strictly decreasing path toward a singular outlet.

b. Floodplain drainage network enforcement

DEMs of flat terrains, as in this study, usually lack the terrain convergence necessary in HAND-SRC (Ghanghas et al., 2022; Godbout et al., 2019). Additionally, the presence of dense vegetation or artificial structures, hinders the delineation of the floodplain drainage network in high-resolution DEMs. Therefore, a hydro-conditioning process was implemented to enforce a micro-drainage network in the floodplain. It consisted of:

(1) Detecting the inherent natural drainage network from the HRDEM using GeoNet tool (Passalacqua et al., 2012). GeoNet, an open-source tool, is mainly used to extract hydrological and morphological data from high-resolution DEMs to detect a network channel, even in the presence of engineered features such as culverts. It was further tested in flat engineered landscapes and urbanized settings (Passalacqua et al., 2010; Sangireddy et al., 2016). The tool detects channelized DEM grid cells based on a Laplacian curvature computation and the flow accumulation area. The drainage network is then delineated based on a geodesic least-cost path algorithm.

(2) Removing pits/sinks to prevent alterations in the flow direction grid.

(3) Enforcing the detected drainage network upon the DEM through a fill-burn tool to preserve the flow direction (Lindsay, 2016; Saunders, 1999).

This process is necessary to: (a) conform to the assumption A1 of the model (see section 3.1.2), (b) minimize the errors caused by the pit filling process in HAND raster calculation (see section 3.1.1) and (c) eliminate drainage discontinuities that arise in the area separating the DEM and the superimposed bathymetries.

c. Removal of levees

In the Ostouane floodplain, levees disrupt the assumption that the floodplains should be draining into the river channel (see section 3.1.2). The existing levee system, installed by locals, is discontinuous and unregulated, failing to effectively mitigate floods. Previous studies have tried to enforce levees into DEMs where the resolution failed to represent these features (Afshari et al., 2018; Aristizabal et al., 2023) whereas here, their influence is investigated by removing the existing levees to restore the channel-floodplain connection.

Levees were detected using an embankment mapping tool (Lindsay, 2016) based on a search distance algorithm that requires the levee's centerline, side slope, height and width, to identify its extent. Due to the variability of levee sizes in our DEM, a set of values covering the range of the measured dimensions of existing levees were iterated (heights between 0.3 and 1.8 m; width between 3 and 10 m). The detected embankments were then replaced by interpolated surfaces from the surrounding elevations.

d. Definition of terrain setups

Several DEMs were developed to assess HAND raster and the HAND-SRC model. Terrain setup S1 is based on the original 25-cm HRDEM. The other terrain setups (S1-rb, S1-fp, S2, S3) are based on the same HRDEM but incorporate additional hydro-conditioning processes, as synthesized in Table 2. Specifically, the surveyed river bathymetry and flowline enforcement are incorporated in terrain setups S1-rb and S2, while the trapezoidal bathymetry is used in terrain setup S3. The floodplain drainage network was enforced in terrain setups S1-fp, S2 and S3. Moreover, levees were removed to finalize terrain setups S2 and S3.

Table 2. Terrain setups used for the assessment of hydro-conditioning and man-made features; × marks the applied configuration in a setup

Terrain setup	River bathymetry	Levee removal

	Original 25-cm HRDEM	Surveyed cross-sections	Trapezoidal power law cross-sections	Floodplain drainage enforcement	
S1	x				
S1-rb	x	x			
S1-fp	x			x	
S2	x	x		x	x
S3	x		x	x	x

427

428 **3.1.4. Sensitivity analysis of reach length parameter**

429 The reach length *L* and Manning's roughness coefficient *n* are the two parameters dictating the model
430 performance. Since Manning's roughness coefficient is established for different land cover types, the
431 reach length parameter was scrutinized as it can be more critical for the accuracy of hydraulic geometry
432 and SRCs (Gordon et al., 2023). A sensitivity analysis was performed using terrain setup S2 since it had
433 the highest level of hydro-conditioning while admitting a high terrain accuracy. Reach lengths adopted in
434 the literature ranged between 1 km and 3 km (Aristizabal et al., 2023; Garousi-Nejad et al., 2019; Hocini
435 et al., 2020; Rebolho et al., 2018; Zheng et al., 2018a, 2018b). *L* values tested here were 150 m, 300 m,
436 600 m, 900 m, and 1350 m and 2700 m.

437 **3.1.5. Testing the effect of DEM resolution**

438 In flood mapping, there are two key attributes of a DEM: the vertical accuracy and the horizontal
439 resolution. In flat terrains, the vertical accuracy can be more significant than the horizontal resolution,
440 with coarser DEMs still capable of reproducing the elevations accurately. However, both attributes are
441 necessary for accurate terrain representation. Using hydraulic models, fine resolution DEMs produce
442 more accurate flood maps and extents compared to coarser ones, even when admitting the same vertical
443 accuracy (Saksena & Merwade, 2015). Whereas using HAND-SRC model, it is generally found that finer
444 resolutions improve performance, however, no clear trend is established across different resolutions. An
445 improvement was found from increasing DEM resolution from 10 m to 3 m by Garousi-Nejad et al.
446 (2019). Conversely, no significant change in the accuracy of inundation extents was registered from
447 varying DEM resolution between 3 and 20 m, but a significant decline was found from using coarser
448 resolutions of 60 and 90 m by Aristizabal et al. (2024). Terrain-based models heavily rely on the DEM as
449 the main input, making them heavily prone to the DEM properties and errors. The variation in DEM
450 resolution leads to increased errors in the vertical accuracy, horizontal accuracy and the representation of
451 artificial features, albeit with lower computational demand. Typically, DEM errors arise from the
452 collection method, sampling methods, interpolation techniques and hydro-conditioning processes.

In this study, the errors stemming from DEM resampling were examined to determine their effect on HAND-SRC model performance. The HAND-SRC was simulated for resolutions of 1m, 3m, 5m, 10m, 20m and 30m which correspond to the most commonly used DEM resolutions. The DEMs were resampled using bilinear interpolation technique from the HRDEM of terrain setup S2. For the sake of comparison between the various resolutions, a fixed reach length *L* of 1.35 km was used. This value was selected due to its suitability for coarser resolutions and as it falls within the adopted range in the literature. The resampled resolutions were evaluated in comparison to the 25-cm HRDEM of setup S2 also using the same *L*.

3.2. Hydraulics-based flood mapping: HEC-RAS

A one-dimensional (1D) hydraulic model was used to develop reference flood maps using a more physically-based approach, for comparison against the low-complexity HAND-SRC model.

3.2.1. Model overview

HEC-RAS (Hydrologic Engineering Center's River Analysis System) is a well-documented and widely used software in fluvial flooding simulation (USACE, 2020). In 1D configuration, the terrain is represented through a series of cross-sections and the flow is assumed to move in a longitudinal direction along the river.

Within a HEC RAS project file, three input files are needed: (1) a geometry file which includes the DEM, the surveyed cross-sections, and Manning's roughness coefficients, (2) a plan file specifying the simulation settings and (3) a steady/unsteady flow file containing the boundary conditions of the model.

3.2.2. Input data, parameters and boundary conditions

The original 25-cm HRDEM was imported as the main input in the geometry file. The river centerline and bank lines were digitized using drone imagery within the RAS-mapper module of HEC-RAS. Cross-sections were then added at the locations of the surveyed ones. The cross-section elevations were corrected using the surveyed point measurements.

The channel Manning's roughness coefficients were determined for each cross-section according to the methodology described in (USDA, 2012), based on field observations, captured photos and drone imagery. For the floodplain, Manning's roughness coefficients were estimated based on the land use/cover maps. Furthermore, the upstream and downstream boundary conditions were set as the normal depth based on the average local slope. The flow file was designated to run the model in a steady state gradually varied flow simulation.

3.2.3. Flood mapping and aggregated rating curves

The HEC RAS model was implemented over a 15 km length of the Ostouane River (see reach A-B in fig. 1b) and simulated for the January 2019 flood. The model's Manning's roughness parameters were calibrated using the available flow records and crowdsourced flood depths. The flood maps at the peak of the January 2019 flood were generated.

A series of rating curves were extracted at all cross-sections. The HEC RAS generated rating curves are valid at the location of cross-sections whereas the SRCs are valid over a river reach. To facilitate comparison between both rating curves, those of HEC RAS were aggregated for cross sections within the same reach. This was achieved by extracting the median of heights at each reach to plot an aggregated rating curve (ARC).

3.3. Evaluation approach and metrics

The evaluation was conducted against: crowdsourced data and HEC RAS flood maps. The former consists of flood occurrences (flooded/non-flooded occurrences) and flood depths.

3.3.1. Comparison of crowdsourced and simulated flood occurrences

To evaluate the model's accuracy in capturing crowdsourced flood occurrences, the contingency table metrics were utilized. The metrics rely on the true positives (TP), false positives (FP), false negatives (FN) and true negatives (TN) values. TP and TN refer to points correctly classified as flooded or non-flooded respectively. FP are non-flooded points falsely classified as flooded. Conversely, FN are flooded points falsely classified as non-flooded by the model.

The critical success index (CSI_P) and Matthews correlation coefficient (MCC_P) metrics were selected to assess the occurrence of flood at these locations. The CSI metric ranges between 0 and 1 while MCC ranges between -1 and 1. For both, a value of 1 represents a perfect match. CSI disregards true negatives and gives more significance to the ability of the model to avoid misses of flooded points or false alarms at non-flooded ones. However, CSI is sensitive to unbalanced datasets. MCC was thus introduced as it provides a balanced score that takes into account all instances of the confusion matrix regardless of their size.

$$CSI_P = \frac{TP_P}{TP_P+FP_P+FN_P} \quad (4)$$

$$MCC_P = \frac{TP_P \times TN_P - FP_P \times FN_P}{\sqrt{(TP_P+FP_P)\times(TP_P+FN_P)\times(TN_P+FP_P)\times(TN_P+FN_P)}} \quad (5)$$

3.3.2. Comparison of simulated flood extents

The simulated flood extents of HAND-SRC and HEC RAS were also compared. CSI and MCC metrics were also utilized but for comparison of simulated areas. For this reason, the two metrics were denoted as CSI_A and MCC_A for HEC RAS maps comparison as opposed to CSI_P and MCC_P used for crowdsourced points. Generally, while evaluating flood maps, CSI values below 0.5 are considered poor while ones above 0.65 are considered good, whereas MCC is considered satisfactory for values above 0.3 (Bernhofen et al., 2018; Fleischmann et al., 2019).

$$CSI_A = \frac{TP_A}{TP_A+FP_A+FN_A} \quad (6)$$

$$MCC_A = \frac{TP_A \times TN_A - FP_A \times FN_A}{\sqrt{(TP_A+FP_A)\times(TP_A+FN_A)\times(TN_A+FP_A)\times(TN_A+FN_A)}} \quad (7)$$

3.3.3. Comparison of crowdsourced and simulated flood depths

The simulated flood depth and the crowdsourced flood depths were compared. The mean absolute error (MAE) and root mean square error (RMSE) were utilized for flood depth error evaluation. The two metrics were also used to calculate the error in DEM vertical accuracy and SRC accuracy.

$$RMSE = \sqrt{\frac{\sum_{i=1}^{n}(depth_{HAND-SRC} - depth_{crowdsourced})^2}{n}} \quad (8)$$

$$MAE = \frac{1}{n}\sum_{i=1}^{n}|depth_{HAND-SRC} - depth_{crowdsourced}| \quad (9)$$

3.3.4. Comparison between simulated flood depths

Flood depths simulated using HAND-SRC and HEC RAS were also compared. Three metrics were used to assess the difference in the depth variable. The mean difference (MD), mean absolute difference (MAD) and the root mean square difference (RMSD) were utilized in this assessment.

$$MD = \frac{1}{n}\sum_{i=1}^{n}(depth_{HEC\ RAS} - depth_{HAND-SRC}) \quad (10)$$

$$MAD = \frac{1}{n}\sum_{i=1}^{n}|depth_{HEC\ RAS} - depth_{HAND-SRC}| \quad (11)$$

$$RMSD = \sqrt{\frac{\sum_{i=1}^{n}(depth_{HEC\ RAS} - depth_{HAND-SRC})^2}{n}} \quad (12)$$

3.4. Workflow and analysis

In our workflow (Fig. 3): (1) the datasets were acquired, assessed and processed including topography and crowdsourced data, (2) terrain setups were developed based on the chosen hydro-conditioning criteria in Table 2 and the resolutions in selected in section 3.1.5, (3) the HAND raster files and SRCs plots were calculated and flood maps were generated for the January 2019 event using the framework described in section 3.1.1, (4) HEC RAS hydraulic model was set up and simulated to derive the flood maps and ARCs, (5) the performance of the flood maps was evaluated against the crowdsourced data and HEC RAS extents.

The methodology used to apply HAND-SRC models here is similar to the one used by (Zheng et al., 2018a). However, several key modifications to the DEM preparation approach were introduced. Specifically, two bathymetric inputs based on the surveyed riverbed and a hydraulic geometry power law were integrated. In addition, a novel hydro-conditioning processes in the bathymetry and floodplain to enforce drainage and remove levees were implemented. A sub-meter high-resolution DEM was utilized for enhanced detection of the natural drainage patterns. This paper is set out to test HAND-SRC flood mapping based on: the terrain representation enhanced by the hydro-conditioning processes and the influence of the DEM resolution.

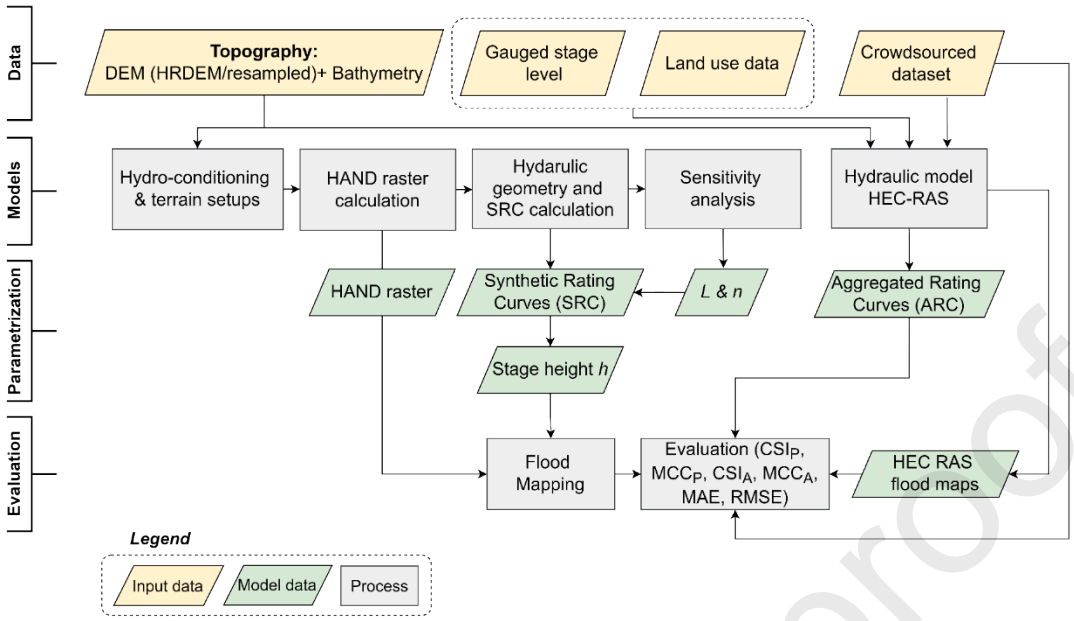

Figure 3: Workflow chart summarizing the main processes involved in the assessment of the HAND-SRC model. The workflow begins with data acquisition followed by development of the terrain setups of HAND-SRC and the HEC RAS model, then the calculation of the HAND raster and SRC plots. Finally, flood maps are generated and evaluated against crowdsourced data and HEC RAS flood maps

4. Results

This section presents the outcome of the study from three aspects: (1) the evaluation of the model terrain analysis and parametrization, (2) the HAND-SRC flood mapping performance compared to crowdsourced points and HEC RAS, and (3) the effect of DEM resolution on flood mapping accuracy and computation time.

4.1. HAND-SRC model evaluation

4.1.1. Effect of hydro-conditioning on HAND raster

The automatic pit filling and drainage delineation in the HAND raster calculation (described in section 3.1.1) can induce significant changes in the DEM. Prior to calculating the HAND raster, the hydro-conditioning processes were applied to prepare the DEMs (see table 2). These processes are also necessary to ensure that the DEM conforms to the assumptions of the HAND-SRC model, which is not naturally achieved with fine resolution DEMs. Figure 4 illustrates the effects of hydro-conditioning procedures on HAND raster (described in section 3.1.3) at four zoomed-in locations. In figure 4a, the riverbed lacking an enforced flowline in terrain setup S1 was filled and flattened leading to the loss of most bathymetric geometry. Enforcing a flowline as in the S1-rb setup (Fig. 4b) allowed retaining most of the topographic details of the channel bathymetry at the expense of minor DEM alterations. Figures 4c and 4d highlight the role of using a fill-burn approach after enforcing a flowline (ex. setup S1-rb), particularly in locations where two or more parallel flowlines coexist leading to a ‘wall-effect’ in the HAND raster (ex. setup S1). This problem is often found in reaches with wide and shallow channels and where river islands are present. In addition, the hydro-conditioning of the floodplains by enforcing a drainage network delineated using GeoNet improved the accuracy of the natural drainage that is influenced by the existing canals and ditches. Consequently, this step reduced the impact of DEM pit

filling as shown in terrain setup S1-fp (figure 4e, 4f). Figures 4g & 4h demonstrate the effect of the combined effect of the three applied processes including the removal of levees in setup S2. The effect of the applied processes is reflected in the expansion of the extent of the HAND raster in addition to the preservation of its terrain accuracy. The talweg profile in the bathymetry of both setups S2 and S3 showed little difference in elevations (Fig. SM3 in supplementary material).

Based on different hydro-conditioning configurations, it was evident that combining all processes is necessary at several locations along the river but especially at the model's test zone (Fig. 1c). Figure 5 illustrates the HAND raster extents using the various terrain setups. The HAND raster of terrain setup S1 (see Table 2) failed to extend over all inundation-prone zones within the floodplain due to the presence of levees. However, hydro-conditioning the floodplain allowed the HAND raster to partially expand into the full flood zone in setups S1-fp, S2 and S3. While integrating bathymetry did not affect the HAND raster extents, removing levees enabled full hydrological continuity in the floodplains. By removing levees that acted as drainage barriers, the HAND raster extended across the full floodplain area on both banks. This comprehensive approach of hydro-conditioning by integrating bathymetry, enforcing floodplain drainage and removing levees, allowed the model to accurately depict the full inundable extent of the terrain across both banks. In the following sections, terrain setups S2 and S3 are scrutinized as they provided HAND rasters with the most accurate representation of the topography and matched the full flood zone extents.

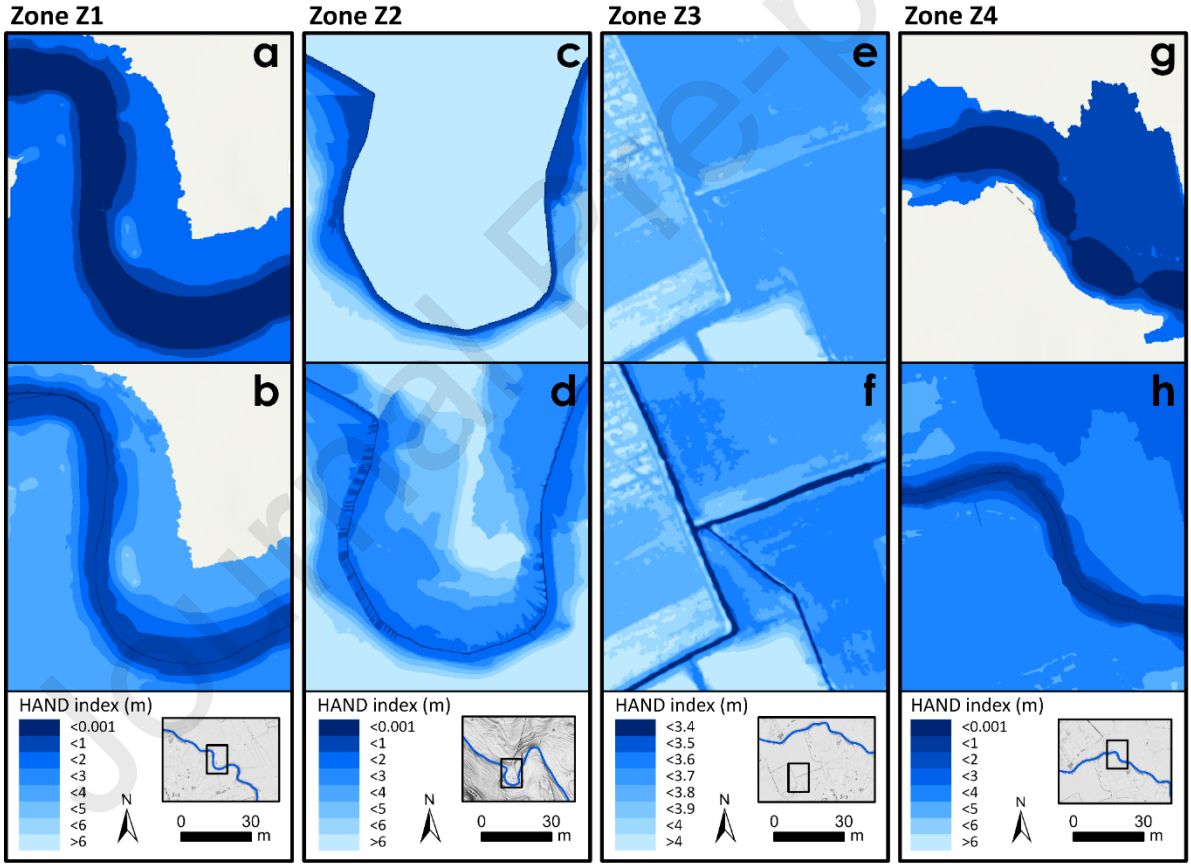

Figure 4: HAND raster maps developed using the HRDEM at four locations: Z1, Z2, Z3 and Z4 highlighting different terrain setups: (a) S1, (b) S1-rb, (c) S1, (d) S1-rb, (e) S1, (f) S1-fp, (g) S1 and (h) S2. (a) & (b) illustrate the impact of flowline enforcement in the bathymetry. (c) & (d) demonstrate the impact of the fill-burn process in preventing a “wall-effect” in the HAND raster. (e) & (f) show the

impact of floodplain drainage enforcement. (g) & (h) illustrate the full impact of bathymetry integration, drainage enforcement and removal of levees

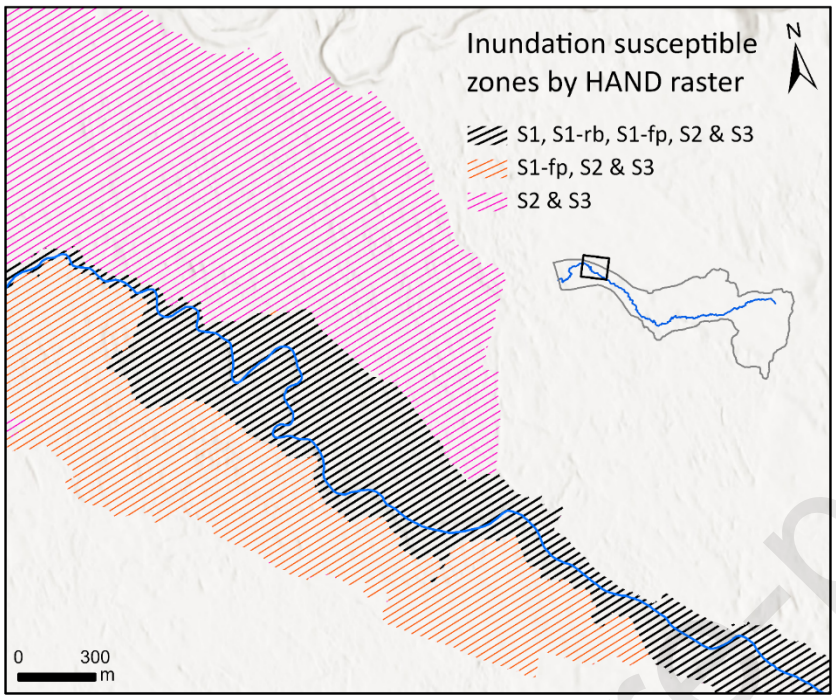

Figure 5: Inundation susceptible zones based on HAND raster extent under the five terrain-setups: S1, S1-rb, S1-fp, S2 and S3 at the test site. S1 includes levees and lacks any hydro-conditioning process, S1-rb includes bathymetry and levees, S1-fp includes levees with floodplain drainage enforcement, S2 includes surveyed bathymetry with floodplain drainage enforcement and no levees, S3 includes surveyed bathymetry with floodplain drainage enforcement and no levees

4.1.2. Model parameterization and sensitivity analysis

Flood mapping using HAND-SRC is highly sensitive to the stage height in flat terrains (Johnson et al., 2019; Jafarzadegan et al., 2022). The reach length L is usually fixed for the entire implementation domain of HAND-SRC. It is generally recommended to use a moderate length between 1.2 and 5 km (Godbout et al., 2019; Zheng et al., 2018a). This is to prevent the effects of local variability in slope and terrain in smaller lengths and the loss of topographic details in lengthier ones. Similarly, Manning's roughness coefficient is applied uniformly over the whole domain. The values are chosen either on the basis of other model parameters or on the basis of land use. The range of this parameter varies between 0.05 and 0.08 $s/m^{1/3}$ (Aristizabal et al., 2023; Garousi-Nejad et al., 2019; Hocini et al., 2020; Johnson et al., 2019; Zheng et al., 2018a). Based on this a Manning's roughness coefficient of 0.07 $s/m^{1/3}$ was selected for the tested domain.

The role of reach length L was investigated by fixing Manning's roughness coefficient n to 0.07 $s/m^{1/3}$ and calculating stage heights for tested reach lengths of 150, 300, 600, 900 and 1350 m. The setup S2 was chosen for the sensitivity analysis as it produced a HAND raster extended to the full floodplain area unlike setups S1, S1-fp and S1-rb, while maintaining the highest topographic accuracy after implementing the hydro-conditioning processes and integrating the surveyed bathymetry. Stage heights were derived from SRCs of each catchment using the estimated peak discharge Q_p=94.1 m^3/s of the January 2019 event. Figure 6 shows the variation in stage value using various reach lengths. Stage heights for L of 150

m and 300 m demonstrated a good ability to capture the crowdsourced flood depths. However, *L* showed little influence on the ability to correctly detect flooded and non-flooded crowdsourced occurrences. A reach length *L* of 300 m was chosen for flood mapping purposes as it showed fewer outlier stage heights arising from topographic heterogeneity compared to *L* = 150 m. In addition, it yielded the lowest RMSE (68.3 cm) compared to other L values.

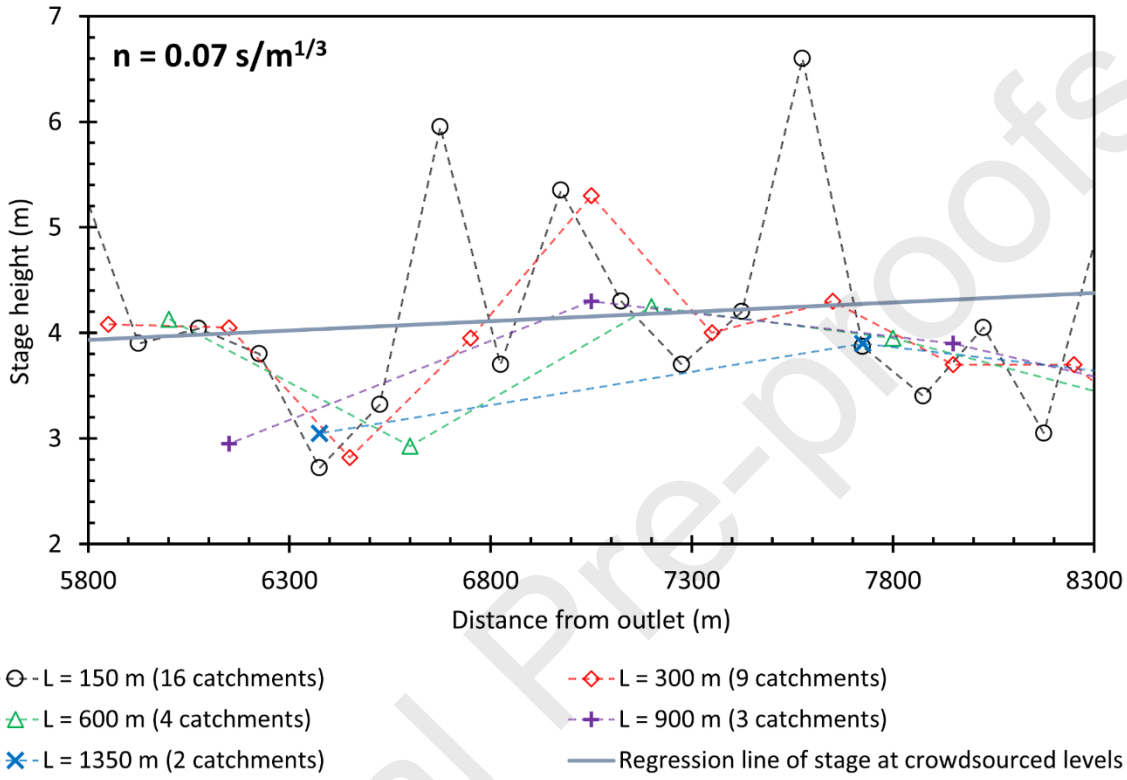

Figure 6: Sensitivity analysis of reach length *L* in the HAND-SRC model. The stage heights (*h*) were calculated for five *L* values in the test site using a fixed Manning's roughness coefficient (n=0.07 s/m$^{1/3}$) and using the peak discharge of January 2019 flood, Q_p. The stage height is referenced to the flowline of each reach and is added on the graph at the midpoint of the reach. A regression line was calculated from the stage heights at which the crowdsourced flood levels are reached

4.2. HAND-SRC flood mapping

4.2.1. Flood depth and occurrence comparison against crowdsourced data

The performance of HAND-SRC flood mapping was investigated against crowdsourced data using the two terrain setups S2 and S3 at the test site at the downstream part of the floodplain (Fig. 1c). The two setups were selected for this assessment because they were the only ones to produce a HAND raster that extends over the full floodplains and preserves a topographic consistency with the original HRDEM after implementing the hydro-conditioning processes. The site has an average DEM slope of 6.7%, a standard deviation of 1.34 m and a river gradient of 0.2%. A reach length of 300 m and a uniform Manning's roughness coefficient n=0.07 s/m$^{1/3}$ were used. By using RMSE, CSI_p and MCC_p an evaluation form that targets the depth and ability to capture the flooded crowdsourced points is elected rather than a flood area. This allows for a more critical review of the model's ability to capture detailed locations within the

floodplain. The validity of crowdsourced data is thus relied upon rather than an established or simulated flood map. The depth comparison made here is between the HAND-SRC flood depths and the crowdsourced flood depths. The latter was calculated as the difference between the surveyed ground elevation and the crowdsourced elevation of peak flood depth. The vertical elevation error was thus not propagated throughout the rest of the calculations.

Figure 7 shows the flood maps generated for the different terrain setups. The figure was generated based on stage heights derived from SRCs of each catchment for Q_p=94.1 m^3/s. The maps have distinct patterns and areas of inundation. The two setups S2 and S3 showed a balanced flooding area over the two banks of the river. Differences between S2 and S3 can be identified where S3 showed higher flood levels and a wider extent compared to S2. Both terrain setups were able to capture the flooded points to a good degree, however S3 submerges several non-flooded points. Terrain setup S2 produced a CSI_P value of 0.64 compared to a CSI_P of 0.79 for S3. Whereas for MCC_P, the results showed values of 0.49 and 0.24 respectively. Additionally, both setups showed a RMSE of 70 cm and 54 cm respectively. Furthermore, an intercomparison between the flood depths obtained with terrain setups S2 and S3 was performed. The mean difference between both was 16 cm with S3 showing a higher flood depth. The mean absolute error amounted to 31.1 cm. While varying level of differences could be observed along the different river reaches, the difference throughout the floodplains was minimal.

The results of both scenarios using the various tested reach lengths are shown in table 3. For all lengths, S2 showed higher RMSE compared to S3. Similarly, the CSI_P metric was also higher using S3. However, for MCC_P, the results were variable with S2 showing higher value except for the 900 m and 2700 m reach lengths. Considering that S2 is a better realization of the bathymetric geometry, S3 with a more simplified geometry showed better metrics in capturing crowdsourced points compared to S2 under most *L* values. This suggests that using a theoretical bathymetry instead of a surveyed one can be sufficient in such applications with minimal difference in flood depths (< 25 cm).

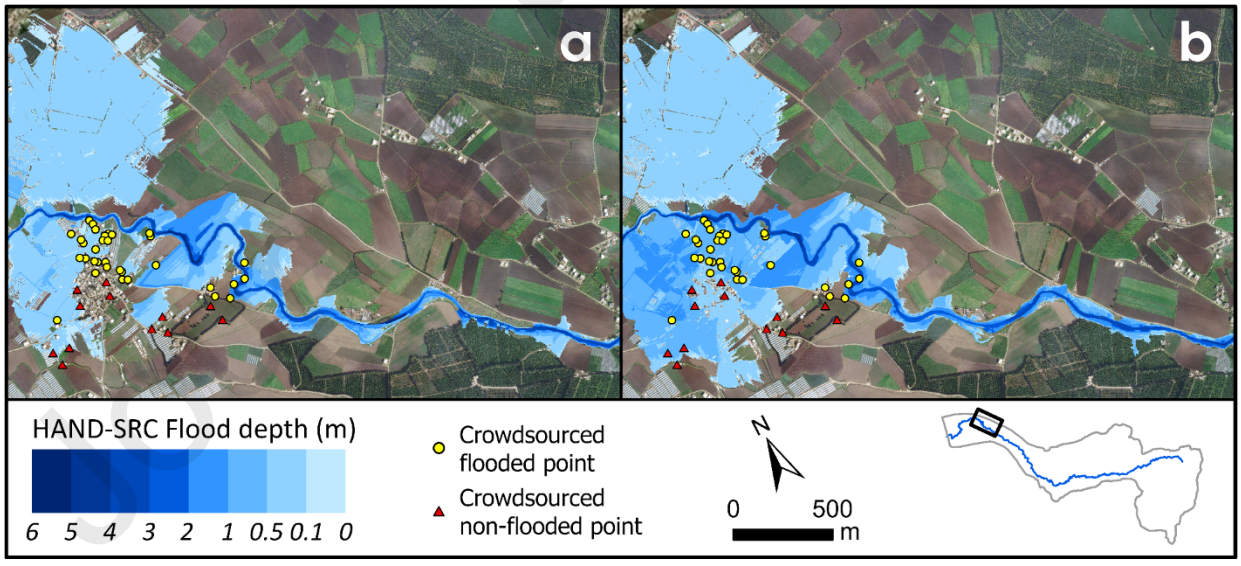

Figure 7: Comparison between simulated HAND-SRC flood maps for the peak discharge Q_p of January 2019 flood event using the 25-cm HRDEM for the two terrain setups: (a) S2, which includes interpolated surveyed bathymetry, flowline and floodplain drainage enforcement, and no levees; and (b) S3, which includes trapezoidal power law cross-section bathymetry, flowline and floodplain drainage enforcement, and no levees. For both setups a reach length of 300 m was used and a Manning's roughness coefficient of n=0.07 $s/m^{1/3}$

Table 3: Terrain setups used for the assessment of hydro-conditioning and man-made features; × marks the applied configuration in a setup

Terrain setup		Reach length L (m)					
		150	300	600	900	1350	2700
S2	RMSE (m)	0.64	0.70	0.71	0.65	0.62	0.61
	CSI_P	0.48	0.64	0.54	0.56	0.63	0.55
	MCC_P	0.38	0.49	0.40	0.41	0.47	0.41
S3	RMSE (m)	0.57	0.54	0.59	0.65	0.55	0.59
	CSI_P	0.75	0.79	0.53	0.53	0.50	0.53
	MCC_P	0.36	0.24	0.18	0.49	0.30	0.49

4.2.2. Flood depth and extent comparison against HEC RAS

The comparison between HAND-SRC and HEC RAS flood maps was conducted for the peak discharge value of the 2019 event for terrain setups S2 and S3 (fig. SM4 in supplementary material). It should be mentioned that the DEM used in HEC RAS does not use the same hydro-conditioned terrain used in HAND-SRC modelling. Instead, it relies on the original HRDEM with corrected cross sections (see section 3.2). Initially, HEC-RAS flood maps were evaluated against crowdsourced points. HEC RAS produced a CSI_P value of 0.61 and the lowest RMSE in flood depth of 34 cm among all tested simulations.

Figure 8 shows the comparison between HAND-SRC inundation maps using S3 setup with the HEC RAS model. Evaluating setup S3 flood extents against HEC RAS extents produced a CSI_A of 0.59 and MCC_A of 0.32. An overprediction by HAND-SRC was found on the left bank of the river contrary to an underprediction on the right bank. For terrain setup S2, HAND-SRC gave a comparable pattern to that of terrain setup S3, with a CSI_A and MCC_A of 0.66 and 0.35 between the two flooded extents. Moreover, the flood depths simulated by HAND-SRC and HEC RAS were compared across overlapping flooded areas. Figure 9 shows the comparison of HEC RAS and HAND-SRC flood depths using terrain setups S2 and S3. In both cases, HAND-SRC underestimated the simulated flood depth. However, setup S2 showed lower errors compared to S3. Terrain setup S2 revealed a MD of 0.15 m, MAD of 0.62 m, and a RMSD of 0.72 m. Whereas under setup S3 a MD of 0.37 m was registered, a MAD of 0.66 m, and a RMSD of 0.98 m. The MD between S2 and S3 was 0.16 m.

699 An alternative approach to simulate flood maps was then tested by using HAND raster of terrain setup S2
700 with ARCs instead of SRCs. The generated flood map showed the highest metric performances, with a
701 CSI_A of 0.86 and MCC_A of 0.65. However, there was generally an overestimation in HEC-RAS depths
702 and extents compared to HAND-SRC. This test demonstrates that a hydro-conditioned terrain setup can
703 replicate the extents simulated by a hydraulic model more accurately by adjusting the reach length and
704 Manning's roughness coefficient parameters.

705 In the operational use of low-complexity models, correctly predicting flood occurrences with minimal
706 misses is essential, therefore, the model parameters were optimized using CSI metric. Testing this, an
707 optimal CSI_P value of 0.73 for crowdsourced data was obtained for a minimum stage height of 4.5 m
708 under all tested reach lengths. Back calculating Manning's roughness coefficient using this stage height
709 produced a corresponding value of $n = 0.095$ s/m$^{1/3}$. Applying this value for all catchments in setup S2
710 improved the performance of the HAND-SRC extents compared to HEC RAS simulated extents by
711 10.6% (CSI_A score 0.66 to 0.73). In contrast, using a Manning's roughness coefficient based on fitting the
712 SRC to the ARC at the Pont Halba gauge station produced a value $n = 0.062$ which hindered the model
713 prediction accuracy in the floodplains downstream.

714 Overall, both terrain setups S2 and S3 showed similar and good agreement with HEC-RAS flood maps.
715 These tests highlight the potential of HAND-SRC model, particularly with hydro-conditioned terrain and
716 optimized parameters. While HEC RAS produced the lowest RMSE in crowdsourced data, the HAND-
717 SRC model was capable of reproducing the HEC RAS extents sufficiently. This demonstrates that even in
718 challenging topographies, the HAND-SRC model can still be reliable for floodplain mapping.

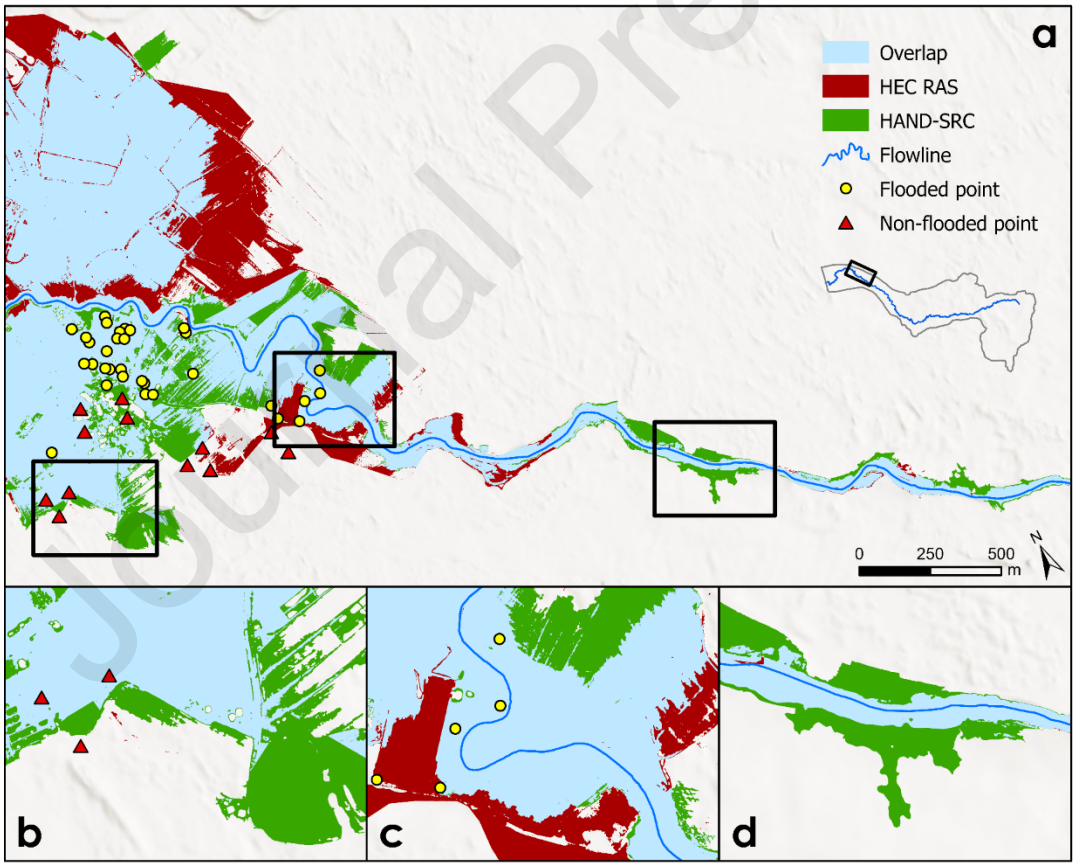

719

720 Figure 8: (a) Comparison of simulated HEC RAS and HAND-SRC extents for the January 2019 flood
721 event using terrain setup S3, (b) zoomed-in extent at the edge of the flood zone, (c) zoomed-in extent at a
722 river meander, and (d) zoomed-in extent in a reach with a deep straight channel

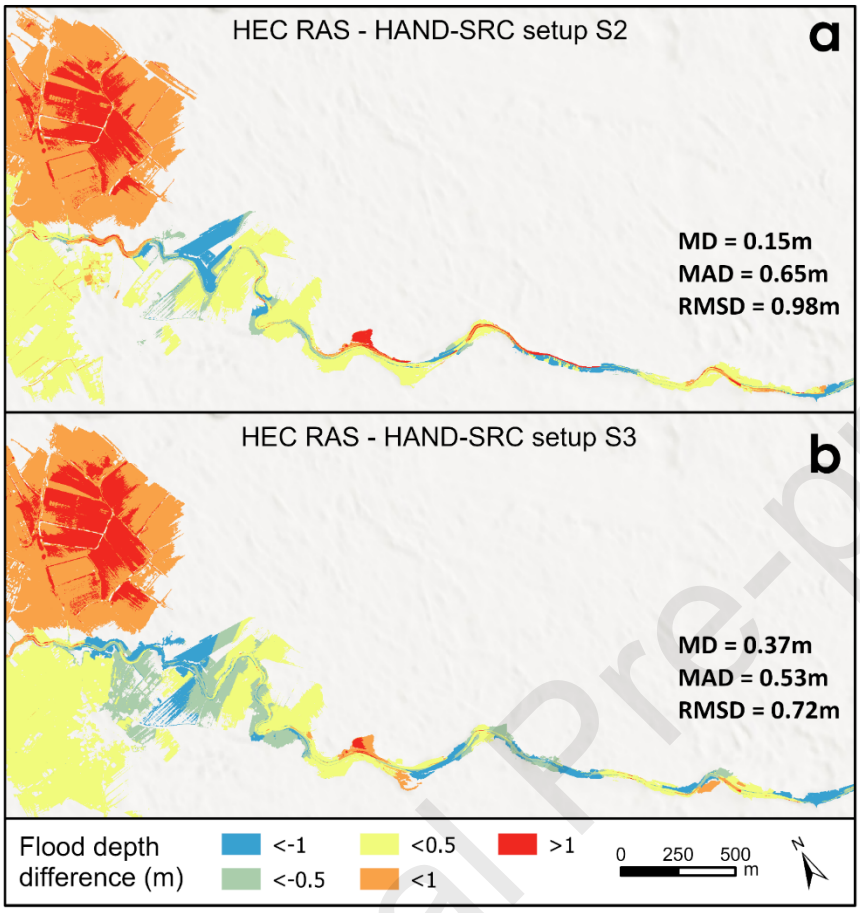

723

724 Figure 9: Comparison of simulated flood depths between HEC RAS and HAND-SRC at test site. The
725 maps were computed by subtracting HEC RAS flood depth from HAND-SRC flood depths for terrain
726 setups: (a) S2 and (b) S3. MD denotes Mean Difference; MAD denote Mean Absolute Difference; and
727 RMSE denote Root Mean Squared Difference

728 **4.3. Resolution effect on HAND-SRC in low-relief areas**

729 **4.3.1. Flood mapping using upscaled resolution**

730 The analysis of the resampled DEMs focuses on the horizontal resolution impact, which is significant on
731 the computational burden and the adherence to the HAND-SRC assumptions. Obtaining high resolution
732 DEMs is still a challenge in many areas, therefore, testing whether coarser resolutions can reproduce
733 similar results is needed from an operational perspective. By resampling the HRDEM enables assessing
734 this effect.

735 Figure 10 illustrates the flood maps at different resolutions. The 1 m resolution DEM produced a similar
736 flood extent and depth to that of the 25 cm HRDEM, yielding a balanced estimate of flood spatial extent.
737 However, the 3 m and 5 m resampled resolutions both showed flooding only on one side of the river. This
738 issue originated from the change in the flow direction grid caused by resampling. At a resolution of 5 m

and above the influence of the natural drainage in the floodplains becomes less significant as the drainage controlling features become dissolved within the grid cells whose size becomes larger than the width of the present ditches and canals. Contrarily, the delineated river flowline using a resolution of 30 m diverged away from the channel. This resulted in a clear overestimation of flood depth as the DEM turned into a completely flat area. The river's bank-full width varies between 8 and 15 meters and loses much of its elevation accuracy at resolutions of 20 and 30 m. At these two resolutions, SRCs showed higher errors and led to exaggerated stage heights. Consequently, the whole catchments were filled up to their boundaries. Generally, these results reflect how employing high-resolution DEMs is crucial for accurate flood modelling in flat regions, as coarser resolutions fail to capture critical drainage features and result in significant errors in flood extent and depth estimation mainly driven by the disruption of terrain convergence between the channel and floodplains.

Figure 11 shows the produced metrics of CSI_A, CSI_P, and the RMSEs in the DEM vertical accuracy, SRCs, simulated flood depths, and flood surface water elevation (SWE) simulated using HAND-SRC under the selected DEM resolutions. $RMSE_{DEM}$ refers to the DEM vertical accuracy that was calculated in comparison against the original HRDEM (before any resampling). $RMSE_{SWE\text{-}CS}$ was calculated for the HAND-SRC surface water elevation compared to the crowdsourced flood SWE. Likewise, the $RMSE_{FD}$ was calculated between the HAND-SRC flood depths and the crowdsourced flood depths. Moreover, $RMSE_{SRC}$ was calculated against the ARC at each catchment. The evaluated terrain resolutions showed a consistent ability to simulate crowdsourced flooded depths except for the 30 m resolution. However, the tested resolutions showed a random ability to capture crowdsourced flood occurrences and HEC RAS flood extents. The 25 cm resolution yielded satisfactory values in all metrics.

Contrary to expectations, a resolution of 20 m also demonstrated a satisfactory replication of HEC RAS extents and crowdsourced depths and occurrences despite the heightened errors in DEM accuracy. It should be noted that the errors in surface water elevations were more significant compared to the errors in flood depth which can be attributed to the heightened errors in DEM vertical accuracy. Furthermore, the resulting HAND rasters and flood maps failed to accurately capture the depth and hydraulic geometry of the river channel. No linear trend was observed from the resampled DEM flood mapping performance. However, some coarser resampled DEM resolutions could sufficiently capture the extent of flooding and crowdsourced occurrences or depths. Nonetheless, their inherent errors and compromised accuracy make them less ideal compared to finer resolutions with higher vertical accuracy.

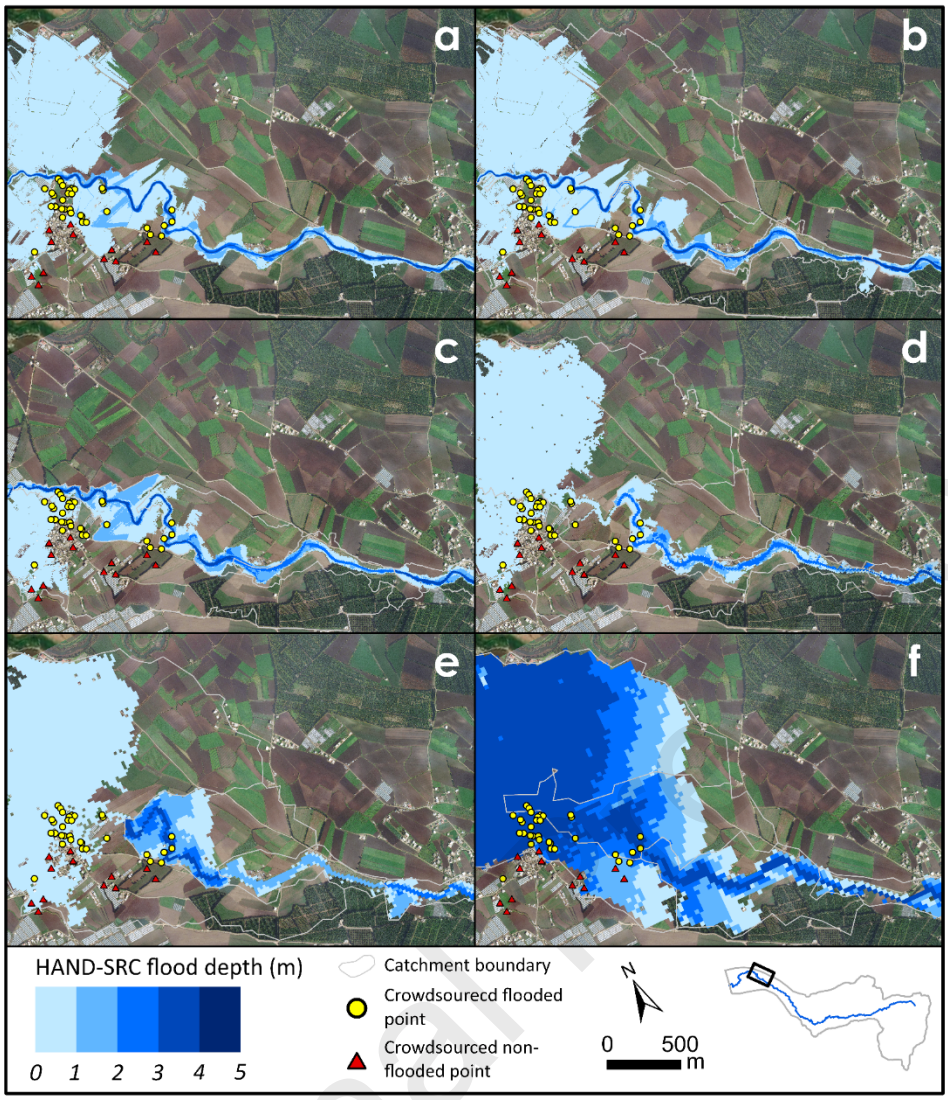

769

770 Figure 10: Simulated HAND-SRC flood maps of the January 2019 flood event using terrain setup S2 at a
771 DEM resolution of (a) 25 cm, (b) 1 m, (c) 5 m, (d) 10 m, (e) 20 m and (f) 30 m. The DEMs were
772 resampled from the 25-cm HRDEM and the reach length used is 1350 m for a constant Manning's
773 roughness coefficient of 0.07

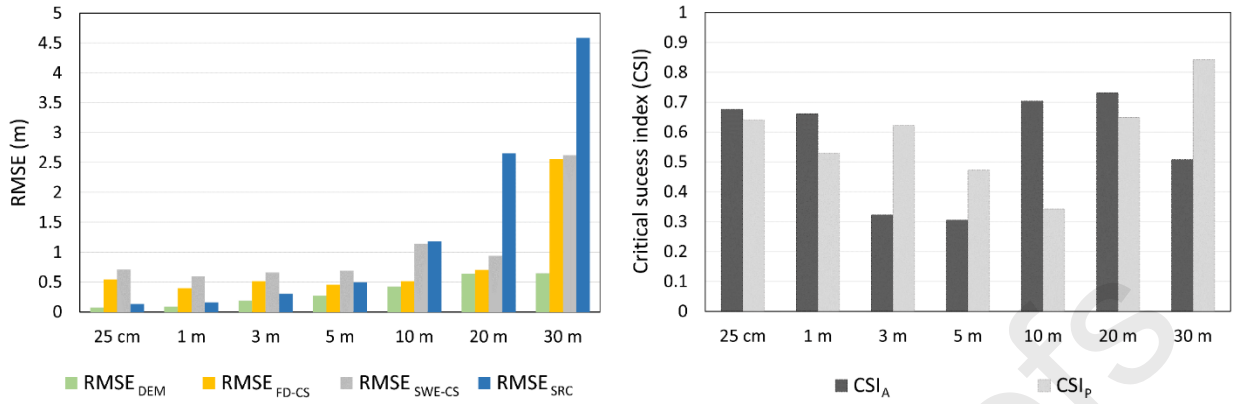

Figure 11: Evaluation of HAND-SRC model using root mean square error (RMSE) and critical success index (CSI) across seven tested resolutions of terrain setup S2. RMSE is calculated for DEM vertical accuracy ($RMSE_{DEM}$), synthetic rating curves (SRCs) compared to ARC ($RSME_{SRC}$), in addition to both crowdsourced flood depth ($RMSE_{FD\text{-}CS}$) and crowdsource ed water surface elevation ($RMSE_{SWE\text{-}CS}$) that were both against HAND-SRC simulations. CSI is calculated for crowdsourced points (CSI_P) and HEC RAS simulated flood extents (CSI_A)

4.3.2.Computation time

The computational time required to run the calculations/simulations showed a large difference between the resampled DEM resolutions (Table 4). A personal computer was used for simulating the HAND-SRC model equipped with an AMD Ryzen 5800h CPU with 8 cores (3.2 GHz and 16 logical processors) in addition to a 16 GB of RAM. Parallel processing was adopted for simulating TauDEM utilities using 16 processes. The total time required to develop the HAND raster and the SRCs using the 25 cm HRDEM with an area of 8 km^2 was 47.4 mins out of which 81% were dedicated for TauDEM utilities. In comparison a 30 m resolution DEM required only 2.1 seconds. Generally, little difference was found when simulating coarse resolutions above 5 m. The 3 m resolution required twice the time compared to the 5 m DEM. Moving from a 3 m to 1 m resolution, a difference of two orders of magnitude in simulation time was observed. An order of magnitude difference was also witnessed when changing the resolution from 1 m to 25 cm resolution. The calculation of HAND raster and SRCs at high resolutions can be of high computational requirement, however it is only needed once. Furthermore, there is no significant computational cost when mapping floods which can be achieved in a matter of a few seconds. In essence, setting up of HAND-SRC may be initially computationally demanding using high resolutions, however, the model is highly efficient for repeated flood simulations required in operational forecasting using all resolutions.

Table 4: The DEM resolutions tested using HAND-SRC, their raster size, uncompressed size and computational time

DEM resolution (m)	Raster Size	Uncompressed size	Computational time (sec)
0.25	17488×15800	1.03 GB	2844.310

1	4372×3938	65.68 MB	100.331
3	1457×1313	7.3 MB	6.811
5	874×788	2.63 MB	3.349
10	437×394	672.57 KB	2.487
20	219×197	168.53 KB	2.158
30	146×131	74.71 KB	2.113

5. Discussion

This section presents the discussion of three aspects that highlights the importance of accurate terrain representation and the challenges of incorporating crowdsourced data sources for flood modelling. Specifically, it covers: (1) the hydro-conditioning processes and the effect of the reach length variation, (2) the flood mapping performance of the model, and (3) the DEM resolution effect on flood mapping.

5.1. Terrain analysis: hydro-conditioning and reach length parameter

Hydro-conditioning is an indispensable practice used to correct or improve the effectiveness of the geometric representation for modelling purposes. The hydro-conditioning processes applied here differ from (Garousi-Nejad et al., 2019; Zheng et al., 2018a) in four ways. First, two bathymetric DEMs were superimposed. The integration of bathymetry is an attempt to ensure topographic accuracy that is consistently absent in similar applications. Second, the enforced flowline was delineated using the D8 approach. Third, the floodplain part of the DEM was hydro-conditioned by enforcing a drainage network delineated using GeoNet. Here, the drainage continuity into a singular flowline was ensured by two drainage enforcement processes, namely the AGREE-DEM and fill-burn processes. Fourth, levees were removed from the DEM to ensure full drainage continuity between the floodplains and river channel, in an unorthodox approach. These hydro-conditioning processes may seem unconventional in hydrological applications but are necessary to adapt to both the terrain's flat nature and the model's assumptions.

A key aspect of integrating interpolated bathymetry is that, unlike the trapezoidal cross-section bathymetry, it may admit multiple parallel flowlines. This generates inconsistencies in the HAND raster due to the increased downstream distance between a DEM grid cell and the flowline grid cell. The flow-burn approach that followed the AGREE DEM approach resolves this limitation, by leading the drainage within the bathymetry into the singular enforced flowline in the HAND raster.

Another pivotal impact of the hydro-conditioning processes is the alteration of the DEM. While this may introduce additional errors, it guarantees drainage continuity through the lowest elevations in the terrain. By enforcing drainage in the bathymetry and floodplain, these processes mitigate the effect of the automatic pit-filling and flow direction grid calculation while preparing the HAND raster. This approach

preserves the consistency between the original DEM and the HAND raster, which is essential for accurate mapping and for comparison with crowdsourced flood levels.

Levee representation within a DEM is highly significant since they act as a barrier against flow. In our study case, the high resolution of the DEM allowed detecting levees that act as a barrier despite their small size. These soil levees, developed through random efforts by local farmers, do not meet modern engineering design standards. They are also scattered along the river course with many gaps and breaches, rendering them non-optimal for flood mitigation. Unlike other studies (Afshari et al., 2018; Aristizabal et al., 2023) that tried to enforce levees into the DEM, we opted to remove them due to their lack of hydraulic significance. Our analysis revealed that removing these levees to allow floodplain drainage into the channel is crucial to producing coherent HAND raster that extend across the complete floodplains (see figure 5) and SRCs that accurately replicate ARCs by maintaining the hydrological connection.

It should be noted that levee presence in a DEM can be highly problematic in HAND-SRC model. Inundation in HAND-SRC is based on traced hydrological connection that drains the floodplains into the channel (assumption A1). These hydrological pathways require a monotonically decreasing flow direction grid that cannot occur in the presence of a levee. Since levees are raised structures that separate two regions in a DEM, no monotonic decrease will be found between the upstream and downstream sides of the levee. Therefore, any traced connection, if found, will be erroneous further contributing to errors in SRC and estimated stage heights. Furthermore, the HAND raster extent, in the presence of a levee, will be restricted to the levee location and will result in an infinite "wall effect" when the raster is filled up to the levee edge. Nonetheless, a stage height can be overlaid over the whole HAND raster regardless of a hydrological connection to overcome the levee problem, as in Afshari et al. (2018). This however, would lead to an overestimation of the flood extent, especially in flat terrains. Another possible workaround can be made by removing the levees and adjusting the SRC such that no floodplain inundation occurs until bank-full discharge is reached.

The two primary parameters of the HAND-SRC model are Manning's roughness coefficient and the reach length L. The former is dependent on the characteristics of the land surface and its features, while several terrain properties dictate the latter. The most commonly used L values in the literature are at least 1000 m. Here, reach lengths down to 150 m were tested. Our analysis revealed an increasing trend in the average stage height when reducing L. The outlier values that appear when using a reach length of 150 m can be attributed to either the delineated catchment's hydraulic geometry or the local slope heterogeneity. Catchments with lower L can be unbalanced, with a larger draining area on one bank of the river or different maximum fillable heights at each bank, leading to a strictly vertical filling of the catchment and consequently an increase in estimated stage heights. This is identified by sudden increasing shifts in SRCs. Reach slope outliers ranging from 0.01% to 0.7% were found in L=150 m, contributing to the stage height variability in some catchments. (Godbout et al., 2019) found that decreasing L below 1.2 km or targeting low-slope reaches reduces SRC accuracy using a 10 m topographic dataset. In our study, the slope and reach length did not show any co-linearity, suggesting that stage height errors using shorter L (< 1000 m) can be mitigated when robust bathymetric measures are available. The limitation on using shorter L remains from the effect of catchment geometry which mainly depends on the terrain connectivity and HAND raster quality.

5.2. HAND-SRC flood mapping

5.2.1. Flood mapping performance

HAND-SRC as a hydrological terrain filling technique coupled with Manning's flow equation lacks the physics of fluid mechanics in more complex hydraulic models using shallow water equations. Manning's flow equation certainly introduces a simplified flow hydraulics representation albeit the limitations

stemming from the uniformity assumption of water levels within a catchment (A3) their discretization along catchments of a river reaches (A4) and the infinite water volume assumption (A5) (see section 3.1.2). These assumptions create a surface water elevation with a stepped curve along the river and fail to conserve mass or momentum across consecutive river reaches. Nonetheless, a plethora of other simplified low-complexity models can be used for rapid flood inundation mapping such as RFSM, TVD, AutoRoute, planar surface, bathtub method, topographic wetness index, geomorphic flood index and slope position (Dhote et al., 2023; Jafarzadegan et al., 2023; Teng et al., 2019). Yet, HAND tends to perform similarly or better than other low-complexity models in terms of simulated extent and depth (Afshari et al., 2018; Dhote et al., 2023; Lioi et al., 2020; McGrath et al., 2018). The model is an efficient and less costly alternative to more physically-based models that admit higher ranges of uncertainty (Diehl et al., 2021).

Overall, the hydro-conditioned terrain setups were capable of capturing the extent and depths of crowdsourced data (CSI_P of 0.64 and 0.79) and HEC RAS extents (CSI_A of 0.66 and 0.59). The presence of crowdsourced points in rural areas may be subject to the influence of terrain features. The resulting magnitude of RMSE errors compared to crowdsourced data was generally on the lower side (< 1m), and this can be attributed to the flat geomorphology of the terrain. While HEC RAS attained a lower RMSE (34 cm), terrain setups S2 and S3 showed a low error as well (70 cm and 54 cm respectively). These values are considered acceptable for flood modelling (Fleischmann et al., 2019).

Interestingly, the trapezoidal bathymetry in S3 produced some enhanced metric performances compared to the surveyed interpolated one in S2 against crowdsourced data (table 3). A slight improvement was also found in replicating HEC RAS extents. Flood depths using S3 were also overestimated against HEC RAS but with similar hot-spots of overestimation and underestimation compared to S2. S3 had lower MAD and RMSD compared to S2 but a higher MD indicating higher outliers than in S2. This implies a greater bias toward underestimation of flood depth in setup S3 compared to setup S2. The average trapezoidal bathymetry area is similar to that of the surveyed interpolated one while both terrains produced similar rating curves. Yet, two main factors influencing this difference can be attributed. (1) The enhanced drainage continuity between the channel with superimposed bathymetry and the floodplain caused by reduced noise and errors resulting from bathymetric interpolation that may create obstructions between both. (2) The reduced errors stemming from the internal drainage within the riverbed that can lead to increased hydrological distance between the flowline and a DEM cell consequently leading to an overestimation of HAND values and therefore reduced flood depths and extents. Such errors arise from possible river islands or from the rectangular delineated drainage pattern within the surveyed interpolated bathymetry. This suggests that a simplified geometry can be more favorable for terrain-based HAND-SRC applications.

5.2.2. Underprediction in low-reliefs

In general, HAND-SRC maps underestimated the flood depths compared to crowdsourced data despite a relatively high Manning's roughness coefficient (n = 0.07 s/m$^{1/3}$). Such a finding was also reported by (Afshari et al., 2018; Hocini et al., 2020). Other works suggested a reduction of Manning's roughness coefficient in high-stream order reaches and low-relief terrains (Johnson et al., 2019). Four factors can be behind this difference. First, the hydro-conditioning can increase the fillable volumes and subsequently, the cross-sectional area implying a higher n is needed as a result of assumption (A5). Second, errors in the river slope in DEMs lacking bathymetry can lead to irregular slope estimates and increased height differences especially in coarser resolutions adopted in the literature. Third, the underestimation of hydraulic geometry due to the lack of bathymetry and the coarse resolutions in the different literature (Godbout et al., 2019; Hocini et al., 2020; Johnson et al., 2019) result in a flat SRC with little sensitivity to elevation. Lastly, the traced hydrological flow path along the flow direction between the flowline cell and a DEM cell may not correspond to the actual distance in reality. This can be due to DEM errors or incorrect drainage delineation resulting in increased distance along the hydrological flow path leading to

increased HAND index at a DEM cell that in reality should be lower. This may further contribute to the underprediction in flat areas.

5.2.3. Perspectives on crowdsourced data

Crowdsourcing introduces a type of uncertainty that is complex to outline and constrain. The source of uncertainty varies according to the type of data, collection method and analysis approach. Yet, the approaches and protocols to understand them are still being developed (Assumpção et al., 2018; Nardi et al., 2022). In our study, the uncertainty in crowdsourced data manifests in the spatiotemporal characterization, originating from the timing of peak flood observation and the elevation errors. Evaluating this requires a transdisciplinary analysis incorporating demographic, social and psychological sciences to deal with the biases and randomness of human observations.

The validation of crowdsourced data relies on external inputs such as remote sensing or aerial imagery at the time of the flood which were not available in our study (Dasgupta et al., 2022; Nardi et al., 2022). Thus, crowdsourced data should adopt structured methods to validate and assess their interoperability without external inputs. The crowdsourced data used here consisted of 45 points of which 33 represented a peak flood water elevation distributed over an area of 0.45 km^2. For rural streams, 5 to 10 high water marks are sufficient to characterize a flood, however, urban settings require a higher number (Koenig et al., 2016). Given the small area of the crowdsourcing survey, the density of the points was found to be sufficient to reduce the uncertainty and eliminate discrepancies. Furthermore, the crowdsourced points were classified into three reliability levels: low, medium and high based on demographic criteria and retrieval abilities of the eyewitness. High and medium reliability points showed a similar level of profile agreement contrary to low reliability points that exhibited a non-linear tendency with several outliers. Interestingly, the complete dataset was capable of providing sufficient information for model validation in the targeted areas. Moreover, the elevation profile from the surveyed flood levels matched the slope and flow direction of the river bed slope (0.16%), showing an agreement with basic hydraulic principles. Therefore, we suggest that an adequate density of crowdsourced points is essential to reduce their associated uncertainty and validate their accuracy.

A main limitation of crowdsourced data is their lack in uninhabited environments and covering urban environments where “sensors” whether human or technological are present. This can produce spatial biases derailing the overall accuracy of the approach in remote areas and agricultural plains. Our dataset admits an unbalance providing dense information only on the left bank of the river. This limitation was significant in the pre-processed terrain setups and tested DEM resolutions (3 m and 5 m) that showed good agreement in CSI_P and RMSE metrics but failed to correctly capture the inundation extent of HEC RAS. Therefore, to overcome this limitation, hydraulic simulations or established flood maps are needed for an overall evaluation of the model on its full domain.

The implementation of HAND-SRC highly depends on the estimation of a stage height. In the literature, different approaches are used including gauged stage levels were used as input (Johnson et al., 2019; Zheng et al., 2018a). In regions suffering from low data availability, alternative sources of information can be used to establish a good range of stages such as remote sensing. In our case limiting the analysis to a single event at its peak can be restricting, however, integrating multiple events may enhance the model's robustness. Crowdsourced data are only fit for local enhancement of the HAND-SRC due to their spatial limitations. Nonetheless, the reliability of the model for a range of discharge values can be enhanced by adjusting the model parameters at each reach until SRCs match the ARCs of a hydraulic model.

The key advantage of using crowdsourced points is that they provide flood depth and extent estimates with minimal acquisition costs, at fine scales, and in urban environments. Yet, this can only be taken advantage of using a DEM with high resolution and accuracy. Integrating the crowdsourced flood depths

964 in calibrating the hydraulic HEC RAS model achieved a low RMSE (34 cm) illustrating the reliability of
965 the dataset and its utility in the absence of other forms of observed data. In the future, crowdsourced data
966 are expected to increasingly complement other forms of observed or remotely sensed data and in data
967 assimilation in flood forecast models.

968 **5.3. DEM resolution requirement in low-reliefs**

969 Low-relief areas are highly prone to floods due to their inherent topographic characteristics. We tested a
970 set of DEMs using HAND-SRC resampled using the bilinear interpolation method. This method was
971 chosen because it preserves the smoothness of the DEM (Haile & Rientjes, 2005). The tests showed that
972 only a 25 cm or a 1 m resolution DEMs can capture both flood depths and extents satisfactorily. The rest
973 of the of coarser resolutions (3 m and above) all showed significant errors in water surface elevation,
974 flood extents or flood depths in channel or floodplain. These errors can be attributed to several factors.
975 First, the resampling of the DEM disrupts the terrain convergence leading to the formation of areas that
976 do not drain into the river channel. This change arising from resampling usually follows no systematic
977 trend (Wu et al., 2008). Second, the change in the drainage patterns results in the filling of the DEM
978 leading to increased errors in the DEM and SRCs. Lastly, the reduction in DEM vertical accuracy is
979 caused by the coarsening effect of the DEM. The first two factors are mostly present in low-relief terrain
980 where resampling does not maintain the flow direction grid or drainage paths. The last factor consists of
981 coarsening errors and errors from the interpolation method which are usually less significant (Muthusamy
982 et al., 2021).

983 Several papers have demonstrated that varying the spatial resolution through resampling has a higher
984 influence on flood depth predictions rather than the extent (Leskens et al., 2014; Saksena & Merwade,
985 2015; Savage et al., 2016) in hydraulic modelling approaches. In our case, HAND-SRC as a terrain-based
986 model showed a random pattern that influenced both the flood extents and depths in flat areas. However,
987 a more comprehensive understanding of the DEM resolution impacts on HAND-SRC requires a broader
988 assessment that includes other topographic settings.

989 Upscaled DEMs from higher resolution DEMs with high vertical accuracy can retain a high accuracy
990 compared to global DEMs (Prakash Mohanty et al., 2020). Therefore, global DEMs may not be reliable
991 for detailed assessment in low-relief sensitive terrains. Whereas, resampled DEMs from high resolution
992 must be used with caution unless it conforms to two factors. (1) The resolution should allow the detection
993 of the natural drainage pattern in the floodplains to achieve terrain convergence. (2) It should maintain
994 enough topographic representation and accuracy in the DEM elevations for precise hydraulic geometry
995 extraction. While an improvement in the performance of resampled DEMs is possible through additional
996 hydro-conditioning, the approaches used in this study do not apply to all tested resolutions and are outside
997 the scope of the study.

998 **6. Conclusion**

999 The purpose of this paper is to study the applicability of the low-complexity terrain-based HAND-SRC
1000 model for flood mapping in a low-relief terrain with developed rural floodplains comprising channels,
1001 ditches and levees. Due to the increasing demand for real time operational forecasting, testing adapted
1002 approaches that provide efficient, rapid and accurate flood maps has become necessary. An application of
1003 the HAND-SRC model using a complete geometric representation at a high resolution was presented. The
1004 study further assessed the effective topographic representation required for HAND-SRC modelling in flat
1005 areas through hydro-conditioning and upscaling DEM resolutions. The implementation was conducted in
1006 the floodplains of the Ostouane catchment in Northern Lebanon. An intensive field investigation was
1007 conducted to acquire a high-resolution DEM (25 cm), the bathymetry and a set of crowdsourced data on a
1008 past flood event. Two sources of model validation were utilized: HEC RAS flood maps and crowdsourced

data that consist of positive/negative flood occurrences and flood depths from a past event. While the first provided a more comprehensive assessment of flood mapping, the latter scrutinized the accuracy of prediction at detailed locations.

Due to the sensitivity of flat terrains and the complexity of detailed floodplain features at high resolutions, an adapted hydro-conditioning approach was introduced to restructure the terrain in preparation for HAND raster and SRC calculations. This is also to adhere to the model assumptions and retain the DEM accuracy. Overall, the terrain setups with the highest level of hydro-conditioning (S2 and S3) showed reasonable prediction performance in capturing crowdsourced flood occurrences (CSI_P of 0.64 and 0.79 respectively), crowdsourced flood depths (RMSE of 0.7 and 0.54 m respectively) and HEC RAS extents (CSI_A of 0.66 and 0.59 respectively). Both setups incorporated drainage enforcement in the bathymetry and floodplain, levee removal, and bathymetric integration. These processes all served the goal of achieving drainage continuity and terrain convergence between the floodplain and the channel. Furthermore, adopting a theoretical bathymetry based on hydraulic geometry power law (S3) produced similar predictions compared to the bathymetry interpolated from surveyed cross-sections (S2). Therefore, a simplified representation of the terrain can still be effective for bathymetry representation.

In addition to the representation of terrain features, the scalability of the hydro-conditioned terrain was evaluated using resampled DEMs. Tested resolutions showed a variable performance mainly driven by the effective topographic structure and properties of the DEM at the different scales. The highest resolutions (25 cm and 1m) performed better in replicating correct flood extents and depths compared to coarser resolutions where effective channel and floodplain features become dissolved. This leads to the loss of drainage continuity and the alteration of terrain convergence in the DEM. Generally, coarser terrains either resampled or from global DEMs should be used with caution due to their inherent structure that does not necessarily conform to the model assumptions in flat terrains. Nonetheless, the utilization of the sub-meter DEM resolution can be highly significant. This is demonstrated by permitting the detection of the natural drainage through the detection of natural and artificial terrain features. The vertical accuracy and fine resolution were both essential in avoiding the perfectly flat surface terrain problem that is commonly found in coarser resolutions. Additionally, it permitted accurately identifying crowdsourced locations and depths with high precision in the DEM. It is worth noting that the use of crowdsourced data allows evaluating the model's ability to capture detailed locations but introduces significant uncertainty and requires placing high credibility in eyewitness accounts. Despite that, such data may be the sole source of model validation in ungauged areas. An adequate density has shown to be necessary for validating the dataset itself without the need to introduce external inputs. The spatial bias of such data however, renders it complementary for modelling validation.

Our results also show that using the hydraulic model's aggregated rating curves (ARCs) instead of synthetic ones (SRCs) demonstrated that the hydro-conditioned terrain can replicate the extents of HEC RAS. Generalizing this finding however, require a more comprehensive review of SRC accuracy for all discharge ranges. Nonetheless, the implemented approach required increasing Manning's roughness coefficient to capture crowdsourced points levels. The fixed assumptions of this parameter can be a limitation of the model but our analysis showed that it can still be locally optimized based on crowdsourced observations.

In conclusion, the HAND-SRC terrain-based model as a continental and regional scale flood mapping approach was found to still be relevant at local scales and in flat terrains. Adopting a high-resolution hydro-conditioned terrain that maintains terrain convergence and drainage continuity, can provide good performance in a challenging low-relief topography. This can be achieved in a simple straightforward fashion compared to hydraulic models that require a more intensive preparation process. The model can be superior in terms of preparation effort and computational time. HAND-SRC cannot be relied on for highly accurate cell by cell estimations of flood depth especially in terrains with anthropogenic features.

However, as a rapid flood mapping model it is capable of providing reasonable satisfactory information on extent and depth. We thus suggest that the model can be beneficial for enhanced rapid identification of flood risk areas and for ensemble-based flood forecast mapping.

Acknowledgement

This research is conducted within a PhD thesis of the first author funded by a bourse from the National Council for Scientific Research in Lebanon (CNRS-L) and the University of Montpellier (UM). The work was conducted in cooperation between the national early warning system platform (NEWSP) in Lebanon, HydroSciences Montpellier (HSM) laboratory, and the laboratory for the study of Soil-Agrosystem-Hydrosystem interactions (LISAH).

Data statement

Data will be made available on request.

CRediT authorship contribution statement

Hassan Sabeh: Conceptualization, Methodology, Investigation, Writing - Original Draft, Writing - Review & Editing. **Chadi Abdallah:** Supervision, Writing - Review & Editing, Funding acquisition, Project administration. **Nanée Chahinian:** Supervision, Writing - Review & Editing. **Marie-George Tournoud:** Supervision, Writing - Review & Editing. **Rouya Hdeib:** Supervision, Writing - Review & Editing. **Roger Moussa:** Conceptualization, Supervision, Writing - Review & Editing

Declaration of competing interest

The authors declare that they have no known competing financial interests or personal relationships that could have appeared to influence the work reported in this paper.

Supplementary material

Table A1. List of abbreviations

Abbreviations	Definition
ARC	Aggregated Rating Curve from HEC RAS model
CSI_A	Critical Success Index used to compare with flood areal extent
CSI_P	Critical Success Index used to compare with crowdsourced points flood occurrences
DEM	Digital Elevation Model
h	Height threshold used for flood mapping in HAND-SRC

HAND	Height Above Nearest Drainage index
HAND-SRC	Flood mapping model based on utilizing HAND index and SRC
HEC RAS	Hydrologic Engineering Center's River Analysis System
HRDEM	High resolution digital elevation model
L	River reach length
MCC_A	Mathew's Correlation Coefficient used to compare with flood area
MCC_P	Mathew's Correlation Coefficient used to compare with crowdsourced points
n	Manning's roughness coefficient
Q_p	Peak flow estimated at Pont Halba (G1) station for 2019 flood event
RMSE	Root Mean Square Error
$RMSE_{DEM}$	Root Mean Square Error of DEM vertical accuracy
$RMSE_{FD-CS}$	Root Mean Square Error in simulated flood depth compared to crowdsourced flood depths
$RMSE_{SRC}$	Root Mean Square Error in synthetic rating curve
$RMSE_{SWE-CS}$	Root Mean Square Error in simulated SWE compared to crowdsourced flood SWE
SRC	Synthetic Rating Curve
SWE	Surface Water Elevation

1078

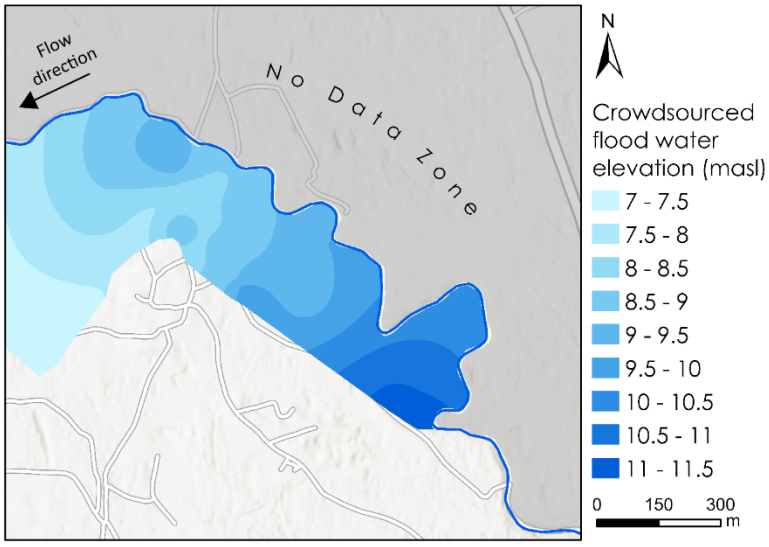

1079

1080 Figure SM1: Delineated flood map using crowdsourced flood depths, flood extent points and non-flooded
1081 point locations

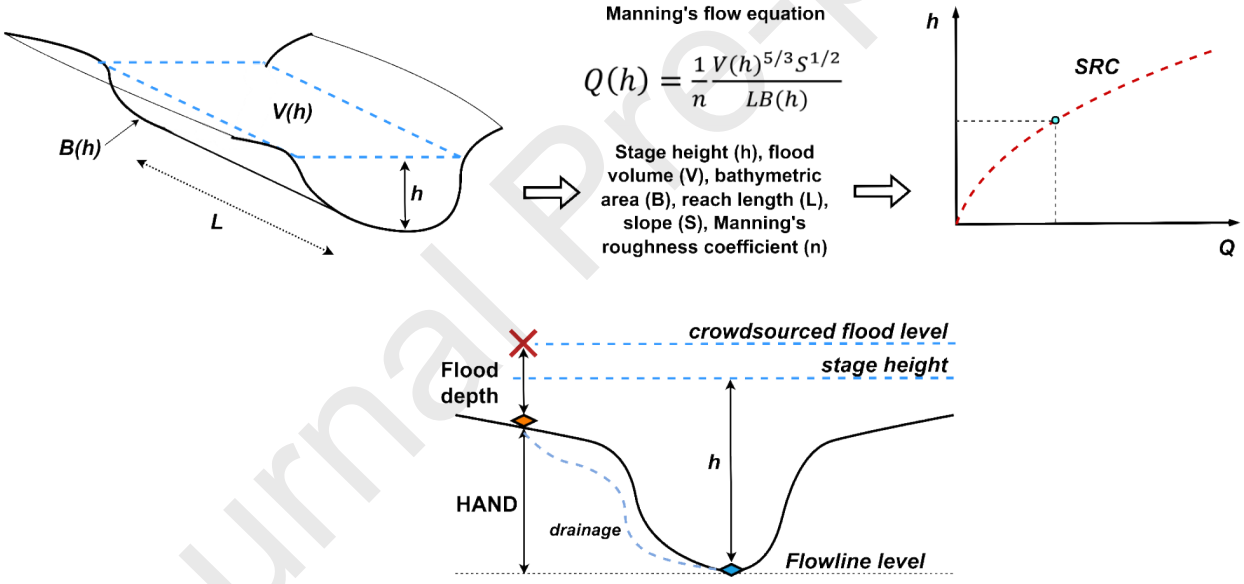

1082

1083 Figure SM2: Illustration of HAND-SRC conceptual model. The HAND raster is filled to a variable stage
1084 height *h* then the hydraulic geometries are extracted. Manning's flow equation is used to estimate the
1085 discharge and plot a synthetic rating curve for a Manning's roughness coefficient

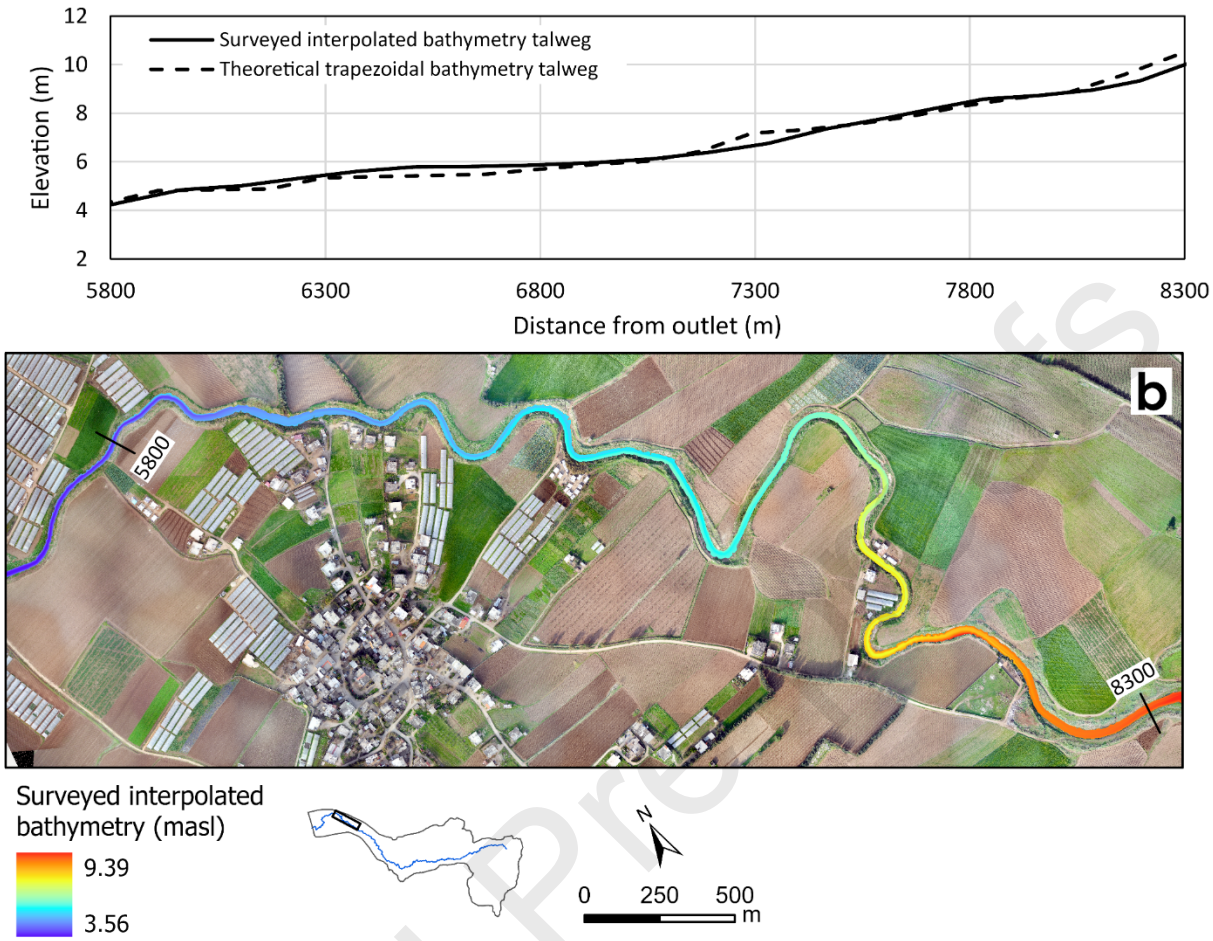

1086

1087 Figure SM3: (a) Talweg elevation in the interpolated surveyed bathymetry and the theoretical trapezoidal
1088 geometry between stations 5300 and 8300 m measured from the river outlet, and (b) bathymetry zone and
1089 elevation across the test site

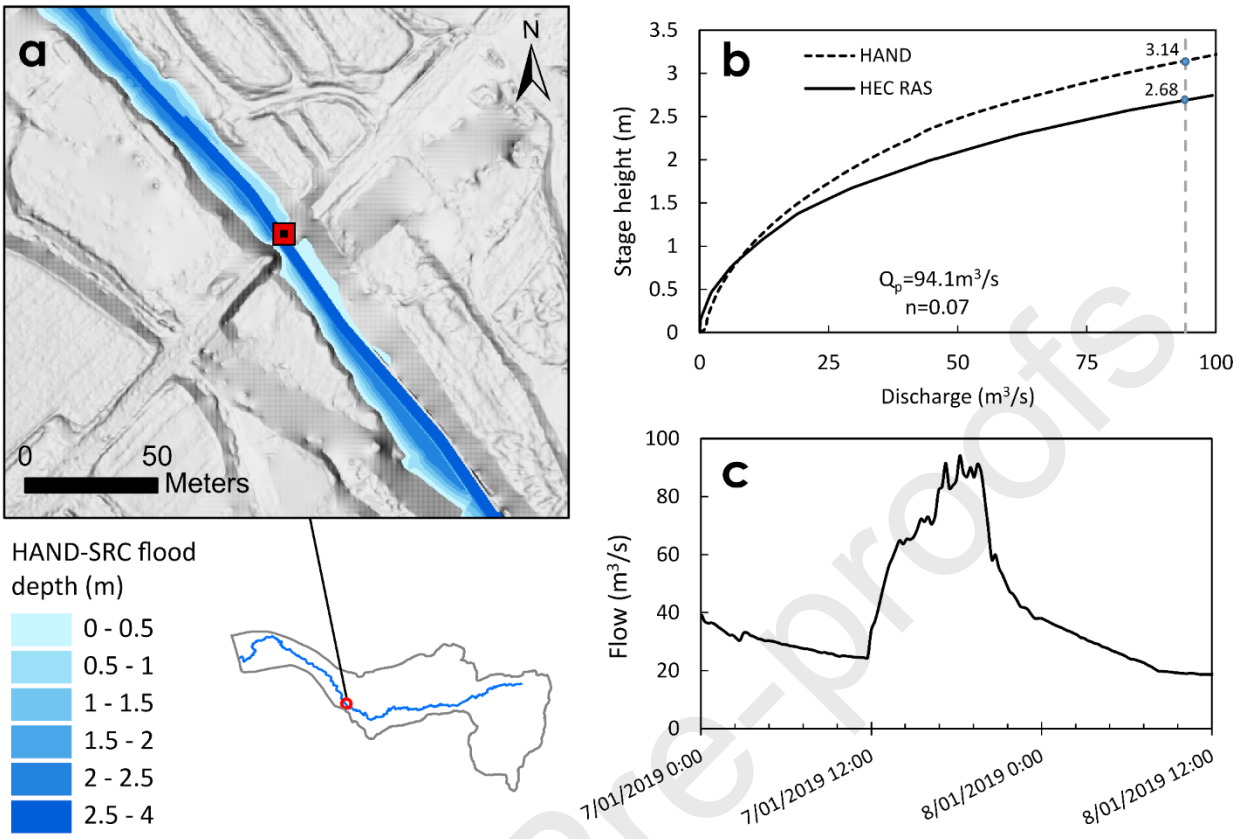

Figure SM4: The January 2019 flood event: (a) HAND-SRC flood depth at Pont Halba gauge station during peak flow; (b) Comparison between SRC and rating curve at the gauge; and (c) flow hydrograph during the event calculated based on the theoretical rating curve

References

Abdallah, C., Hdeib, R., Al Sabeh, H., & Khatib, H. (2023). *FLOOD RISK ASSESSMENT FOR LEBANON "ROFAKA2 AL NAHER PROJECT"* (p. 128P). CNRS-L.

Afshari, S., Tavakoly, A. A., Rajib, M. A., Zheng, X., Follum, M. L., Omranian, E., & Fekete, B. M. (2018). Comparison of new generation low-complexity flood inundation mapping tools with a hydrodynamic model. *Journal of Hydrology*, *556*, 539–556. https://doi.org/10.1016/j.jhydrol.2017.11.036

Annis, A., Nardi, F., Morrison, R. R., & Castelli, F. (2019). Investigating hydrogeomorphic floodplain mapping performance with varying DTM resolution and stream order. *Hydrological Sciences Journal*, *64*(5), 525–538. https://doi.org/10.1080/02626667.2019.1591623

Aristizabal, F., Chegini, T., Petrochenkov, G., Salas, F., & Judge, J. (2024). Effects of high-quality elevation data and explanatory variables on the accuracy of flood inundation mapping via Height Above Nearest Drainage. *Hydrology and Earth System Sciences*, *28*(6), 1287–1315. https://doi.org/10.5194/hess-28-1287-2024

Aristizabal, F., Salas, F., Petrochenkov, G., Grout, T., Avant, B., Bates, B., Spies, R., Chadwick, N., Wills, Z., & Judge, J. (2023). Extending Height Above Nearest Drainage to Model Multiple

Fluvial Sources in Flood Inundation Mapping Applications for the U.S. National Water Model. *Water Resources Research*, *59*(5), e2022WR032039. https://doi.org/10.1029/2022WR032039

Assumpção, T. H., Popescu, I., Jonoski, A., & Solomatine, D. P. (2018). Citizen observations contributing to flood modelling: Opportunities and challenges. *Hydrology and Earth System Sciences*, *22*(2), 1473–1489. https://doi.org/10.5194/hess-22-1473-2018

Bernhofen, M. V., Whyman, C., Trigg, M. A., Sleigh, P. A., Smith, A. M., Sampson, C. C., Yamazaki, D., Ward, P. J., Rudari, R., Pappenberger, F., Dottori, F., Salamon, P., & Winsemius, H. C. (2018). A first collective validation of global fluvial flood models for major floods in Nigeria and Mozambique. *Environmental Research Letters*, *13*(10), 104007. https://doi.org/10.1088/1748-9326/aae014

Beven, K. J., & Kirkby, M. J. (1979). A physically based, variable contributing area model of basin hydrology / Un modèle à base physique de zone d'appel variable de l'hydrologie du bassin versant. *Hydrological Sciences Bulletin*, *24*(1), 43–69. https://doi.org/10.1080/02626667909491834

Buytaert, W., Zulkafli, Z., Grainger, S., Acosta, L., Alemie, T. C., Bastiaensen, J., De BiÃ¨vre, B., Bhusal, J., Clark, J., Dewulf, A., Foggin, M., Hannah, D. M., Hergarten, C., Isaeva, A., Karpouzoglou, T., Pandeya, B., Paudel, D., Sharma, K., Steenhuis, T., … Zhumanova, M. (2014). Citizen science in hydrology and water resources: Opportunities for knowledge generation, ecosystem service management, and sustainable development. *Frontiers in Earth Science*, *2*. https://doi.org/10.3389/feart.2014.00026

CRED. (2022). *CRED - 2022—2021 Disasters in Numbers*. OECD. https://www.oecd-ilibrary.org/economics/inflation-cpi/indicator/english_eee82e6e-en

Darwish, T., Khawlie, M., Jomaa, M., Abou Daher, M., Awad, M., Masri, M., Shaban, A., Faour, G., Bou Kheir, R., Abdallah, C., & Haddad, T. (2006). *Digital Soil Map of Lebanon 1/50,000. Monograph Series 4. CNRS Lebanon.*

Dasgupta, A., Grimaldi, S., Ramsankaran, R., Pauwels, V. R. N., & Walker, J. P. (2022). A simple framework for calibrating hydraulic flood inundation models using Crowd-sourced water levels. *Journal of Hydrology*, *614*, 128467. https://doi.org/10.1016/j.jhydrol.2022.128467

Deiana, C., Deidda, R., & Viola, F. (2023). Geomorphic floodplain mapping in small Mediterranean catchments using LiDAR data. *Advances in Water Resources*, *178*, 104493. https://doi.org/10.1016/j.advwatres.2023.104493

Dhote, P. R., Joshi, Y., Rajib, A., Thakur, P. K., Nikam, B. R., & Aggarwal, S. P. (2023). Evaluating topography-based approaches for fast floodplain mapping in data-scarce complex-terrain regions: Findings from a Himalayan basin. *Journal of Hydrology*, *620*, 129309. https://doi.org/10.1016/j.jhydrol.2023.129309

Diehl, R. M., Gourevitch, J. D., Drago, S., & Wemple, B. C. (2021). Improving flood hazard datasets using a low-complexity, probabilistic floodplain mapping approach. *PLOS ONE*, *16*(3), e0248683. https://doi.org/10.1371/journal.pone.0248683

Dubertret, L. (1945). *Cartes geologiques du Liban a l'echelle de 1/50000.* [Dataset].

Fleischmann, A., Paiva, R., & Collischonn, W. (2019). Can regional to continental river hydrodynamic models be locally relevant? A cross-scale comparison. *Journal of Hydrology X*, *3*, 100027. https://doi.org/10.1016/j.hydroa.2019.100027

Garousi-Nejad, I., Tarboton, D. G., Aboutalebi, M., & Torres-Rua, A. F. (2019). Terrain Analysis Enhancements to the Height Above Nearest Drainage Flood Inundation Mapping Method. *Water Resources Research*, *55*(10), 7983–8009. https://doi.org/10.1029/2019WR024837

Ghanghas, A., Dey, S., & Merwade, V. (2022). Evaluating the reliability of synthetic rating curves for continental scale flood mapping. *Journal of Hydrology*, *606*, 127470. https://doi.org/10.1016/j.jhydrol.2022.127470

Gharari, S., Hrachowitz, M., Fenicia, F., & Savenije, H. H. G. (2011). Hydrological landscape classification: Investigating the performance of HAND based landscape classifications in a central European meso-scale catchment. *Hydrology and Earth System Sciences*, *15*(11), 3275–3291. https://doi.org/10.5194/hess-15-3275-2011

Gitundu, D. T., Gathenya, J. M., Raude, J. M., Sang, J., & Ngugi, H. N. (2023). Hydraulic analysis of flash flood events using UAV based topographic data and citizen science in Enkare Narok river basin. *Remote Sensing Applications: Society and Environment*, *30*, 100977. https://doi.org/10.1016/j.rsase.2023.100977

Godbout, L., Zheng, J. Y., Dey, S., Eyelade, D., Maidment, D., & Passalacqua, P. (2019). Error Assessment for Height Above the Nearest Drainage Inundation Mapping. *JAWRA Journal of the American Water Resources Association*, *55*(4), 952–963. https://doi.org/10.1111/1752-1688.12783

Gordon, C. A., Foulon, E., & Rousseau, A. N. (2023). Deriving synthetic rating curves from a digital elevation model to delineate the inundated areas of small watersheds. *Journal of Hydrology: Regional Studies*, *50*, 101580. https://doi.org/10.1016/j.ejrh.2023.101580

Greenwood, W. W., Lynch, J. P., & Zekkos, D. (2019). Applications of UAVs in Civil Infrastructure. *Journal of Infrastructure Systems*, *25*(2), 04019002. https://doi.org/10.1061/(ASCE)IS.1943-555X.0000464

Grimaldi, S., Petroselli, A., Arcangeletti, E., & Nardi, F. (2013). Flood mapping in ungauged basins using fully continuous hydrologic–hydraulic modeling. *Journal of Hydrology*, *487*, 39–47. https://doi.org/10.1016/j.jhydrol.2013.02.023

Haile, A. T., & Rientjes, T. H. M. (2005). *EFFECTS OF LIDAR DEM RESOLUTION IN FLOOD MODELLING: A MODEL SENTITIVITY STUDY FOR THE CITY OF TEGUCIGALPA, HONDURAS*.

Hamdani, N., & Baali, A. (2019). Height Above Nearest Drainage (HAND) model coupled with lineament mapping for delineating groundwater potential areas (GPA). *Groundwater for Sustainable Development*, *9*, 100256. https://doi.org/10.1016/j.gsd.2019.100256

Hellweger, F. (1997). *AGREE-DEM surface reconditioning system*.

Hocini, N., Payrastre, O., Bourgin, F., Gaume, E., Davy, P., Lague, D., Poinsignon, L., & Pons, F. (2020). *Performance of automated flood inundation mapping methods in acontext of flash floods: A*

comparison of three methods based eitheron the Height Above Nearest Drainage (HAND) concept, or on1D/2D shallow water equations [Preprint]. Catchment hydrology/Modelling approaches. https://doi.org/10.5194/hess-2020-597

Jafarzadegan, K., Moradkhani, H., Pappenberger, F., Moftakhari, H., Bates, P., Abbaszadeh, P., Marsooli, R., Ferreira, C., Cloke, H. L., Ogden, F., & Duan, Q. (2023). Recent Advances and New Frontiers in Riverine and Coastal Flood Modeling. *Reviews of Geophysics*, *61*(2), e2022RG000788. https://doi.org/10.1029/2022RG000788

Jafarzadegan, K., Muñoz, D. F., Moftakhari, H., Gutenson, J. L., Savant, G., & Moradkhani, H. (2022). Real-time coastal flood hazard assessment using DEM-based hydrogeomorphic classifiers. *Natural Hazards and Earth System Sciences*, *22*(4), 1419–1435. https://doi.org/10.5194/nhess-22-1419-2022

Johnson, J. M., Munasinghe, D., Eyelade, D., & Cohen, S. (2019). An integrated evaluation of the National Water Model (NWM)–Height Above Nearest Drainage (HAND) flood mapping methodology. *Natural Hazards and Earth System Sciences*, *19*(11), 2405–2420. https://doi.org/10.5194/nhess-19-2405-2019

Koenig, T., Bruce, J., O'Connor, J., McGee, B., Holmes, R., Hollins, R., Forbes, B., Kohn, M., Schellekens, M., Martin, Z., & Peppler, M. (2016). Identifying and preserving high-water mark data. *U.S. Geological Survey*, *No. A-324*. https://doi.org/10.3133/tm3A24

Lacy, J. W., & Stark, C. E. L. (2013). The neuroscience of memory: Implications for the courtroom. *Nature Reviews Neuroscience*, *14*(9), 649–658. https://doi.org/10.1038/nrn3563

Leskens, J. G., Brugnach, M., Hoekstra, A. Y., & Schuurmans, W. (2014). Why are decisions in flood disaster management so poorly supported by information from flood models? *Environmental Modelling & Software*, *53*, 53–61. https://doi.org/10.1016/j.envsoft.2013.11.003

Lhomme, J., Sayers, P., Gouldby, B., & Wils, M. (2008, October). *Recent development and application of a rapid flood spreading method*. https://doi.org/DOI: 10.1201/9780203883020.ch2

Li, Z., Duque, F. Q., Grout, T., Bates, B., & Demir, I. (2023). Comparative analysis of performance and mechanisms of flood inundation map generation using Height Above Nearest Drainage. *Environmental Modelling & Software*, *159*, 105565. https://doi.org/10.1016/j.envsoft.2022.105565

Lindsay, J. B. (2016). Whitebox GAT: A case study in geomorphometric analysis. *Computers & Geosciences*, *95*, 75–84. https://doi.org/10.1016/j.cageo.2016.07.003

Lioi, B., Gioia, A., Totaro, V., Balacco, G., Iacobellis, V., & Chiaia, G. (2020). Coupled Use of Hydrologic-Hydraulic Model and Geomorphological Descriptors for Flood-Prone Areas Evaluation: A Case Study of Lama Lamasinata. In O. Gervasi, B. Murgante, S. Misra, C. Garau, I. Blečić, D. Taniar, B. O. Apduhan, A. M. A. C. Rocha, E. Tarantino, C. M. Torre, & Y. Karaca (Eds.), *Computational Science and Its Applications – ICCSA 2020* (Vol. 12252, pp. 607–619). Springer International Publishing. https://doi.org/10.1007/978-3-030-58811-3_44

Liu, Y. Y., Maidment, D. R., Tarboton, D. G., Zheng, X., & Wang, S. (2018). A CyberGIS Integration and Computation Framework for High-Resolution Continental-Scale Flood Inundation Mapping.

JAWRA Journal of the American Water Resources Association, *54*(4), 770–784. https://doi.org/10.1111/1752-1688.12660

Malgwi, M. B., Ramirez, J. A., Zischg, A., Zimmermann, M., Schürmann, S., & Keiler, M. (2021). A method to reconstruct flood scenarios using field interviews and hydrodynamic modelling: Application to the 2017 Suleja and Tafa, Nigeria flood. *Natural Hazards*, *108*(2), 1781–1805. https://doi.org/10.1007/s11069-021-04756-z

Manfreda, S., Di Leo, M., & Sole, A. (2011). Detection of Flood-Prone Areas Using Digital Elevation Models. *Journal of Hydrologic Engineering*, *16*(10), 781–790. https://doi.org/10.1061/(ASCE)HE.1943-5584.0000367

Manfreda, S., Nardi, F., Samela, C., Grimaldi, S., Taramasso, A. C., Roth, G., & Sole, A. (2014). Investigation on the use of geomorphic approaches for the delineation of flood prone areas. *Journal of Hydrology*, *517*, 863–876. https://doi.org/10.1016/j.jhydrol.2014.06.009

Mazzoleni, M., Verlaan, M., Alfonso, L., Monego, M., Norbiato, D., Ferri, M., & Solomatine, D. P. (2017). Can assimilation of crowdsourced data in hydrological modelling improve flood prediction? *Hydrology and Earth System Sciences*, *21*(2), 839–861. https://doi.org/10.5194/hess-21-839-2017

McGrath, H., Bourgon, J.-F., Proulx-Bourque, J.-S., Nastev, M., & Abo El Ezz, A. (2018). A comparison of simplified conceptual models for rapid web-based flood inundation mapping. *Natural Hazards*, *93*(2), 905–920. https://doi.org/10.1007/s11069-018-3331-y

Merwade, V., Cook, A., & Coonrod, J. (2008). GIS techniques for creating river terrain models for hydrodynamic modeling and flood inundation mapping. *Environmental Modelling & Software*, *23*(10–11), 1300–1311. https://doi.org/10.1016/j.envsoft.2008.03.005

Mudashiru, R. B., Sabtu, N., Abustan, I., & Balogun, W. (2021). Flood hazard mapping methods: A review. *Journal of Hydrology*, *603*, 126846. https://doi.org/10.1016/j.jhydrol.2021.126846

Muthusamy, M., Casado, M. R., Butler, D., & Leinster, P. (2021). Understanding the effects of Digital Elevation Model resolution in urban fluvial flood modelling. *Journal of Hydrology*, *596*, 126088. https://doi.org/10.1016/j.jhydrol.2021.126088

Nardi, F., Cudennec, C., Abrate, T., Allouch, C., Annis, A., Assumpção, T., Aubert, A. H., Bérod, D., Braccini, A. M., Buytaert, W., Dasgupta, A., Hannah, D. M., Mazzoleni, M., Polo, M. J., Sæbø, Ø., Seibert, J., Tauro, F., Teichert, F., Teutonico, R., … Grimaldi, S. (2022). Citizens AND HYdrology (CANDHY): Conceptualizing a transdisciplinary framework for citizen science addressing hydrological challenges. *Hydrological Sciences Journal*, *67*(16), 2534–2551. https://doi.org/10.1080/02626667.2020.1849707

Nardi, F., Vivoni, E. R., & Grimaldi, S. (2006). Investigating a floodplain scaling relation using a hydrogeomorphic delineation method. *Water Resources Research*, *42*(9), 2005WR004155. https://doi.org/10.1029/2005WR004155

Notti, D., Giordan, D., Caló, F., Pepe, A., Zucca, F., & Galve, J. (2018). Potential and Limitations of Open Satellite Data for Flood Mapping. *Remote Sensing*, *10*(11), 1673. https://doi.org/10.3390/rs10111673

1266 Passalacqua, P., Belmont, P., & Foufoula-Georgiou, E. (2012). Automatic geomorphic feature extraction
1267 from lidar in flat and engineered landscapes. *Water Resources Research*, *48*(3), 2011WR010958.
1268 https://doi.org/10.1029/2011WR010958

1269 Passalacqua, P., Do Trung, T., Foufoula-Georgiou, E., Sapiro, G., & Dietrich, W. E. (2010). A geometric
1270 framework for channel network extraction from lidar: Nonlinear diffusion and geodesic paths.
1271 *Journal of Geophysical Research: Earth Surface*, *115*(F1), 2009JF001254.
1272 https://doi.org/10.1029/2009JF001254

1273 Paul, J. D., Buytaert, W., Allen, S., Ballesteros-Cánovas, J. A., Bhusal, J., Cieslik, K., Clark, J., Dugar, S.,
1274 Hannah, D. M., Stoffel, M., Dewulf, A., Dhital, M. R., Liu, W., Nayaval, J. L., Neupane, B.,
1275 Schiller, A., Smith, P. J., & Supper, R. (2018). Citizen science for hydrological risk reduction and
1276 resilience building. *WIREs Water*, *5*(1), e1262. https://doi.org/10.1002/wat2.1262

1277 Prakash Mohanty, M., Nithya, S., Nair, A. S., Indu, J., Ghosh, S., Mohan Bhatt, C., Srinivasa Rao, G., &
1278 Karmakar, S. (2020). Sensitivity of various topographic data in flood management: Implications
1279 on inundation mapping over large data-scarce regions. *Journal of Hydrology*, *590*, 125523.
1280 https://doi.org/10.1016/j.jhydrol.2020.125523

1281 Rebolho, C., Andréassian, V., & Le Moine, N. (2018). Inundation mapping based on reach-scale effective
1282 geometry. *Hydrology and Earth System Sciences*, *22*(11), 5967–5985.
1283 https://doi.org/10.5194/hess-22-5967-2018

1284 Rennó, C. D., Nobre, A. D., Cuartas, L. A., Soares, J. V., Hodnett, M. G., Tomasella, J., & Waterloo, M.
1285 J. (2008). HAND, a new terrain descriptor using SRTM-DEM: Mapping terra-firme rainforest
1286 environments in Amazonia. *Remote Sensing of Environment*, *112*(9), 3469–3481.
1287 https://doi.org/10.1016/j.rse.2008.03.018

1288 Rentschler, J., & Salhab, M. (2020). *People in Harm's Way: Flood Exposure and Poverty in 189*
1289 *Countries*. The World Bank. https://doi.org/10.1596/1813-9450-9447

1290 Rodda, H. J. E. (2005). The Development and Application of a Flood Risk Model for the Czech Republic.
1291 *Natural Hazards*, *36*(1–2), 207–220. https://doi.org/10.1007/s11069-004-4549-4

1292 Saksena, S., & Merwade, V. (2015). Incorporating the effect of DEM resolution and accuracy for
1293 improved flood inundation mapping. *Journal of Hydrology*, *530*, 180–194.
1294 https://doi.org/10.1016/j.jhydrol.2015.09.069

1295 Samela, C., Troy, T. J., & Manfreda, S. (2017). Geomorphic classifiers for flood-prone areas delineation
1296 for data-scarce environments. *Advances in Water Resources*, *102*, 13–28.
1297 https://doi.org/10.1016/j.advwatres.2017.01.007

1298 Sangireddy, H., Stark, C. P., Kladzyk, A., & Passalacqua, P. (2016). GeoNet: An open source software
1299 for the automatic and objective extraction of channel heads, channel network, and channel
1300 morphology from high resolution topography data. *Environmental Modelling & Software*, *83*, 58–
1301 73. https://doi.org/10.1016/j.envsoft.2016.04.026

1302 Saunders, W. (1999). Preparation of DEMs for Use in Environmental Modeling Analysis. *In: ESRI User*
1303 *Conference*, *pp. 24-30.*

Savage, J. T. S., Pianosi, F., Bates, P., Freer, J., & Wagener, T. (2016). Quantifying the importance of spatial resolution and other factors through global sensitivity analysis of a flood inundation model. *Water Resources Research*, *52*(11), 9146–9163. https://doi.org/10.1002/2015WR018198

Schietti, J., Emilio, T., Rennó, C. D., Drucker, D. P., Costa, F. R. C., Nogueira, A., Baccaro, F. B., Figueiredo, F., Castilho, C. V., Kinupp, V., Guillaumet, J.-L., Garcia, A. R. M., Lima, A. P., & Magnusson, W. E. (2014). Vertical distance from drainage drives floristic composition changes in an Amazonian rainforest. *Plant Ecology & Diversity*, *7*(1–2), 241–253. https://doi.org/10.1080/17550874.2013.783642

Schumann, G. J.-P., Neal, J. C., Voisin, N., Andreadis, K. M., Pappenberger, F., Phanthuwongpakdee, N., Hall, A. C., & Bates, P. D. (2013). A first large-scale flood inundation forecasting model: Large-Scale Flood Inundation Forecasting. *Water Resources Research*, *49*(10), 6248–6257. https://doi.org/10.1002/wrcr.20521

Siebert, S., & Teizer, J. (2014). Mobile 3D mapping for surveying earthwork projects using an Unmanned Aerial Vehicle (UAV) system. *Automation in Construction*, *41*, 1–14. https://doi.org/10.1016/j.autcon.2014.01.004

Songchon, C., Wright, G., & Beevers, L. (2023). The use of crowdsourced social media data to improve flood forecasting. *Journal of Hydrology*, *622*, 129703. https://doi.org/10.1016/j.jhydrol.2023.129703

Sy, B., Frischknecht, C., Dao, H., Consuegra, D., & Giuliani, G. (2019). Flood hazard assessment and the role of citizen science. *Journal of Flood Risk Management*, *12*(S2), e12519. https://doi.org/10.1111/jfr3.12519

Sy, B., Frischknecht, C., Dao, H., Consuegra, D., & Giuliani, G. (2020). Reconstituting past flood events: The contribution of citizen science. *Hydrology and Earth System Sciences*, *24*(1), 61–74. https://doi.org/10.5194/hess-24-61-2020

Tamminga, A. D., Eaton, B. C., & Hugenholtz, C. H. (2015). UAS-based remote sensing of fluvial change following an extreme flood event. *Earth Surface Processes and Landforms*, *40*(11), 1464–1476. https://doi.org/10.1002/esp.3728

Tarboton, D. G. (2024). Terrain Analysis Using Digital Elevation Models (TauDEM). *Utah Water Research Laboratory, Utah State University*. https://hydrology.usu.edu/taudem/taudem5/

Teng, J., Jakeman, A. J., Vaze, J., Croke, B. F. W., Dutta, D., & Kim, S. (2017). Flood inundation modelling: A review of methods, recent advances and uncertainty analysis. *Environmental Modelling & Software*, *90*, 201–216. https://doi.org/10.1016/j.envsoft.2017.01.006

Teng, J., Vaze, J., Kim, S., Dutta, D., Jakeman, A. J., & Croke, B. F. W. (2019). Enhancing the Capability of a Simple, Computationally Efficient, Conceptual Flood Inundation Model in Hydrologically Complex Terrain. *Water Resources Management*, *33*(2), 831–845. https://doi.org/10.1007/s11269-018-2146-7

United States Department of Agriculture (USDA). (2012). *Part 630 Hydrology National Engineering Handbook Chapter 14: Stage Discharge Relations*. https://directives.sc.egov.usda.gov/OpenNonWebContent.aspx?content=31844.wba

1343 USACE. (2020). HEC-RAS River Analysis System Hydrauic Reference Manual version 6.0.
1344 *Hydrological Engineering Center. US Army Corps of Engineers*.

1345 Westoby, M. J., Brasington, J., Glasser, N. F., Hambrey, M. J., & Reynolds, J. M. (2012). 'Structure-
1346 from-Motion' photogrammetry: A low-cost, effective tool for geoscience applications.
1347 *Geomorphology*, *179*, 300–314. https://doi.org/10.1016/j.geomorph.2012.08.021

1348 Wing, O. E. J., Bates, P. D., Neal, J. C., Sampson, C. C., Smith, A. M., Quinn, N., Shustikova, I.,
1349 Domeneghetti, A., Gilles, D. W., Goska, R., & Krajewski, W. F. (2019a). A New Automated
1350 Method for Improved Flood Defense Representation in Large-Scale Hydraulic Models. *Water*
1351 *Resources Research*, *55*(12), 11007–11034. https://doi.org/10.1029/2019WR025957

1352 Wing, O. E. J., Sampson, C. C., Bates, P. D., Quinn, N., Smith, A. M., & Neal, J. C. (2019b). A flood
1353 inundation forecast of Hurricane Harvey using a continental-scale 2D hydrodynamic model.
1354 *Journal of Hydrology X*, *4*, 100039. https://doi.org/10.1016/j.hydroa.2019.100039

1355 Woodrow, K., Lindsay, J. B., & Berg, A. A. (2016). Evaluating DEM conditioning techniques, elevation
1356 source data, and grid resolution for field-scale hydrological parameter extraction. *Journal of*
1357 *Hydrology*, *540*, 1022–1029. https://doi.org/10.1016/j.jhydrol.2016.07.018

1358 Wu, S., Li, J., & Huang, G. H. (2008). A study on DEM-derived primary topographic attributes for
1359 hydrologic applications: Sensitivity to elevation data resolution. *Applied Geography*, *28*(3), 210–
1360 223. https://doi.org/10.1016/j.apgeog.2008.02.006

1361 Yamazaki, D., Ikeshima, D., Sosa, J., Bates, P. D., Allen, G. H., & Pavelsky, T. (2019). MERIT Hydro: A
1362 High-Resolution Global Hydrography Map Based on Latest Topography Dataset. *Water*
1363 *Resources Research*, *55*(6). https://doi.org/doi.org/10.1029/2019WR024873

1364 Zheng, X., D'Angelo, C., Maidment, D. R., & Passalacqua, P. (2022). Application of a Large-Scale
1365 Terrain-Analysis-Based Flood Mapping System to Hurricane Harvey. *JAWRA Journal of the*
1366 *American Water Resources Association*, *58*(2), 149–163. https://doi.org/10.1111/1752-
1367 1688.12987

1368 Zheng, X., Liu, Y. Y., & Passalacqua, P. (2018a). GeoFlood: Large-Scale Flood Inundation Mapping
1369 Based on High-Resolution Terrain Analysis. *Water Resources Research*, *54*(12).
1370 https://doi.org/10.1029/2018WR023457

1371 Zheng, X., Tarboton, D. G., Maidment, D. R., Liu, Y. Y., & Passalacqua, P. (2018b). River Channel
1372 Geometry and Rating Curve Estimation Using Height above the Nearest Drainage. *JAWRA*
1373 *Journal of the American Water Resources Association*, *54*(4), 785–806.
1374 https://doi.org/10.1111/1752-1688.12661

1375

1376 **Highlights:**

1377 • HAND-SRC applied in low-relief terrain with anthropogenic features in North Lebanon

1378 • Adapted hydro-conditioning necessary for HAND-SRC to replicate HEC-RAS flood extents

1379 • Crowdsourced depths are well captured by HAND-SRC (CSI = 0.64 and RMSE = 54 cm)

- Integrated power-law bathymetry can reproduce flood maps of surveyed bathymetry
- High DEM resolution ≤ 1 m maintains terrain convergence for HAND-SRC accuracy

Evaluating Terrain-Based HAND-SRC Flood Mapping Model in Low-Relief Rural

Objective: what is the effective representation of terrain for HAND-SRC flood mapping in a low-relief terrain?

Study Area & Data **Methodology** **Effect of terrain hydro-conditioning** **DEM Resolution effect**

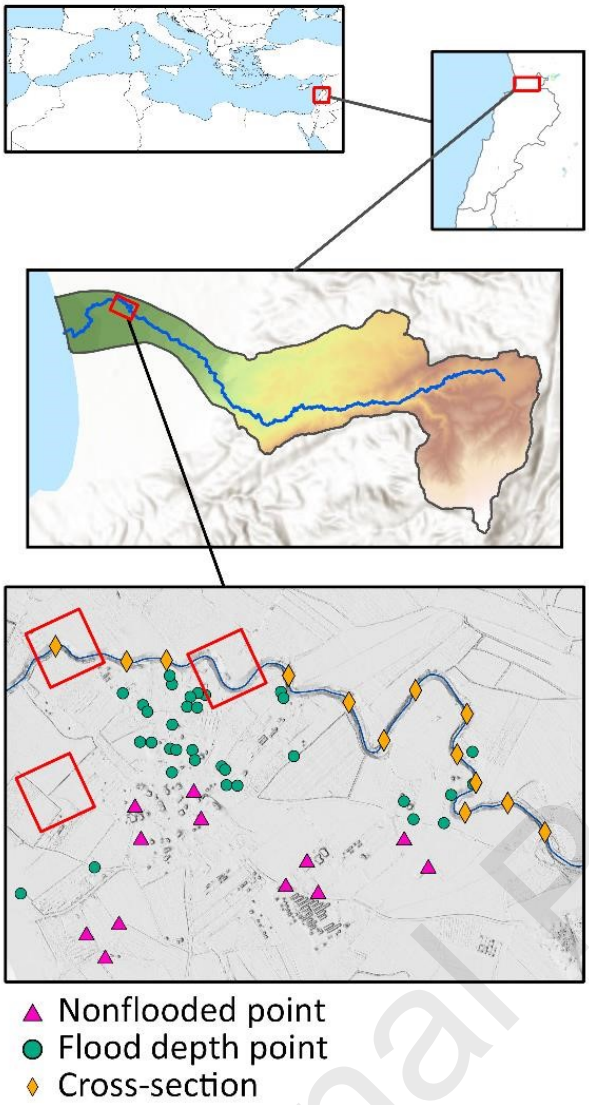

- Drone photogrammetry: 25-cm DEM
- Cross-sections
- Crowdsourcing of 2019 flood event
- Gauged water level
- Land use/cover

1398

1399

HAND-SRC model

HAND index raster

Terrain Hydro-conditioning

1. Integration of surveyed & theoretical bathymetry
2. Bathymetry drainage enforcement
3. Floodplain drainage enforcement
4. Levee removal

Synthetic Rating Curves (SRC)

1. Extraction of hydraulic geometry
2. Sensitivity analysis

Upscaling DEM resolution

1, 3, 5, 10, 20 & 30 m

HEC RAS model

Reference flood maps

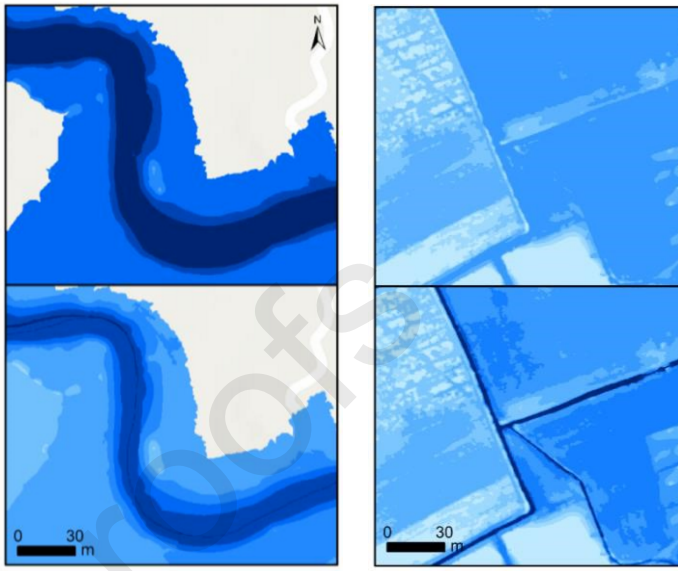

Effect of bathymet

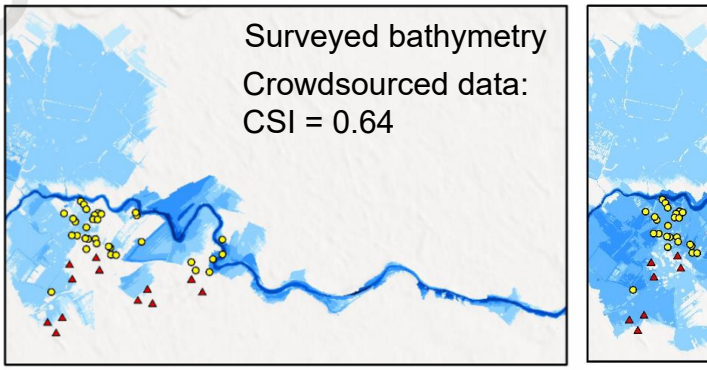

Flood extent comp

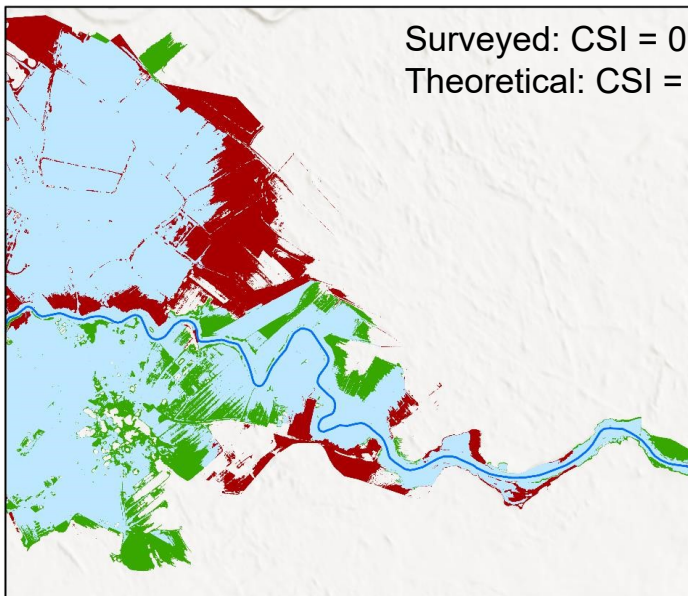

1401